A&A 573, A45 (2015)
DOI: 10.1051/0004-6361/201424937

Astronomy & Astrophysics

The far-infrared/radio correlation and radio spectral index of galaxies in the SFR–M_* plane up to $z \sim 2$⋆

B. Magnelli[1], R. J. Ivison[2,3], D. Lutz[4], I. Valtchanov[5], D. Farrah[6], S. Berta[4], F. Bertoldi[1], J. Bock[7,8], A. Cooray[9], E. Ibar[10], A. Karim[1], E. Le Floc'h[11], R. Nordon[12], S. J. Oliver[13], M. Page[14], P. Popesso[4], F. Pozzi[15], D. Rigopoulou[16,17], L. Riguccini[18], G. Rodighiero[19], D. Rosario[4], I. Roseboom[2], L. Wang[13], and S. Wuyts[4]

[1] Argelander-Institut für Astronomie, Universität Bonn, Auf dem Hügel 71, 53121 Bonn, Germany
e-mail: magnelli@astro.uni-bonn.de
[2] Institute for Astronomy, University of Edinburgh, Blackford Hill, Edinburgh EH9 3HJ, UK
[3] European Southern Observatory, Karl-Schwarzschild-Str. 2, 85748 Garching bei München, Germany
[4] Max-Planck-Institut für extraterrestrische Physik, Postfach 1312, Giessenbachstraße 1, 85741 Garching, Germany
[5] Herschel Science Centre, ESAC, Villanueva de la Cañada, 28691 Madrid, Spain
[6] Department of Physics, Virginia Tech, Blacksburg, VA 24061, USA
[7] California Institute of Technology, 1200 E. California Blvd., Pasadena, CA 91125, USA
[8] Jet Propulsion Laboratory, 4800 Oak Grove Drive, Pasadena, CA 91109, USA
[9] Center for Cosmology, Department of Physics and Astronomy, University of California, Irvine, CA 92697, USA
[10] Instituto de Física y Astronomía, Universidad de Valparaíso, Avda. Gran Bretaña 1111, 5030 Casilla Valparaíso, Chile
[11] Laboratoire AIM, CEA/DSM-CNRS-Université Paris Diderot, IRFU/Service d'Astrophysique, Bât. 709, CEA-Saclay, 91191 Gif-sur-Yvette Cedex, France
[12] School of Physics and Astronomy, The Raymond and Beverly Sackler Faculty of Exact Sciences, Tel Aviv University, 69978 Tel Aviv, Israel
[13] Astronomy Centre, Dept. of Physics & Astronomy, University of Sussex, Brighton BN1 9QH, UK
[14] Mullard Space Science Laboratory, University College London, Holmbury St Mary, Dorking, Surrey RH5 6NT, UK
[15] Dipartimento di Astronomia, Università di Bologna, via Ranzani 1, 40127 Bologna, Italy
[16] Department of Physics, University of Oxford, Keble Road, Oxford, OX1 3RH, UK
[17] RAL Space, Science & Technology Facilities Council, Rutherford Appleton Laboratory, Didcot, OX11 0QX, UK
[18] NASA Ames, Moffett Field, CA 94035, USA
[19] Dipartimento di Astronomia, Università di Padova, Vicolo dell'Osservatorio 3, 35122 Padova, Italy

Received 6 September 2014 / Accepted 21 October 2014

ABSTRACT

We study the evolution of the radio spectral index and far-infrared/radio correlation (FRC) across the star-formation rate – stellar masse (i.e. SFR–M_*) plane up to $z \sim 2$. We start from a stellar-mass-selected sample of galaxies with reliable SFR and redshift estimates. We then grid the SFR–M_* plane in several redshift ranges and measure the infrared luminosity, radio luminosity, radio spectral index, and ultimately the FRC index (i.e. $q_{\rm FIR}$) of each SFR–M_*–z bin. The infrared luminosities of our SFR–M_*–z bins are estimated using their stacked far-infrared flux densities inferred from observations obtained with the *Herschel* Space Observatory. Their radio luminosities and radio spectral indices (i.e. α, where $S_\nu \propto \nu^{-\alpha}$) are estimated using their stacked 1.4 GHz and 610 MHz flux densities from the Very Large Array and Giant Metre-wave Radio Telescope, respectively. Our far-infrared and radio observations include the most widely studied blank extragalactic fields – GOODS-N, GOODS-S, ECDFS, and COSMOS – covering a total sky area of ~2.0 deg^2. Using this methodology, we constrain the radio spectral index and FRC index of star-forming galaxies with $M_* > 10^{10}\,M_\odot$ and $0 < z < 2.3$. We find that $\alpha^{1.4\,{\rm GHz}}_{610\,{\rm MHz}}$ does not evolve significantly with redshift or with the distance of a galaxy with respect to the main sequence (MS) of the SFR–M_* plane (i.e. $\Delta\log(SSFR)_{\rm MS} = \log[SSFR({\rm galaxy})/SSFR_{\rm MS}(M_*, z)]$). Instead, star-forming galaxies have a radio spectral index consistent with a canonical value of 0.8, which suggests that their radio spectra are dominated by non-thermal optically thin synchrotron emission. We find that the FRC index, $q_{\rm FIR}$, displays a moderate but statistically significant redshift evolution as $q_{\rm FIR}(z) = (2.35\pm0.08)\times(1+z)^{-0.12\pm0.04}$, consistent with some previous literature. Finally, we find no significant correlation between $q_{\rm FIR}$ and $\Delta\log(SSFR)_{\rm MS}$, though a weak positive trend, as observed in one of our redshift bins (i.e. $\Delta[q_{\rm FIR}]/\Delta[\Delta\log(SSFR)_{\rm MS}] = 0.22 \pm 0.07$ at $0.5 < z < 0.8$), cannot be firmly ruled out using our dataset.

Key words. galaxies: evolution – galaxies: formation – galaxies: starburst – galaxies: high-redshift – infrared: galaxies

1. Introduction

The far-infrared (FIR) and radio luminosities of star-forming galaxies are tightly related via an empirical relation, the FIR/radio correlation (FRC; e.g. de Jong et al. 1985; Helou et al. 1985, 1988; Condon 1992; Yun et al. 2001). In the local Universe, this FRC is roughly linear across three orders of magnitude in luminosity, $10^9 \lesssim L_{\rm IR}(8{-}1000\,\mu{\rm m})\,[L_\odot] \lesssim 10^{12.5}$, from dwarf galaxies to ultra-luminous infrared galaxies (ULIRGs; $L_{\rm IR} > 10^{12}\,L_\odot$). At lower luminosities, the FRC exhibits some signs of non-linearity (e.g. Bell et al. 2003). The FRC not only

⋆ *Herschel* is an ESA space observatory with science instruments provided by European-led Principal Investigator consortia and with important participation from NASA.

exists on galactic scales but also holds in star-forming regions within the galaxies, down to at least 0.5 kpc, albeit with some variations, as shown by resolved studies of nearby galaxies (e.g. Beck & Golla 1988; Bicay & Helou 1990; Murphy et al. 2008; Dumas et al. 2011; Tabatabaei et al. 2013a,b).

The FRC is thought to be caused by star-formation activity in galaxies. Young massive stars ($\gtrsim$8 $M_\odot$) radiate most of their energy at UV wavelengths, photons that dominate the UV continuum luminosity of galaxies and which are absorbed and re-emitted in the FIR regime by dust. After several Myrs, these young massive stars explode as supernovae (SNe), accelerating cosmic rays (CRs) into the general magnetic field of their host galaxy and resulting in diffuse synchrotron emission. Averaged over a star-formation episode, massive stars thus provide a common origin for the FIR and synchrotron emission of galaxies. This shared origin is the essence of all models constructed to explain the FRC on both global scales (e.g. the calorimeter model, Völk 1989; the conspiracy model, Lacki et al. 2010) and local scales (e.g. small-scale dynamo, Schleicher & Beck 2013; see also Niklas & Beck 1997). While many of these models are able to reproduce the basic properties of the FRC, none are consistent with all constraints provided by observations.

Despite our lack of a thorough theoretical understanding, the very tight empirical FRC (with a dispersion of ~0.25 dex; e.g. Yun et al. 2001) has been used extensively for a number of astrophysical purposes. For example, the FRC observed in the local Universe has been exploited to empirically calibrate the radio luminosity as a star-formation rate (SFR) indicator, using the known $L_{\rm IR}$-SFR relation for galaxies whose activities are not dominated by active galaxy nuclei (AGN; e.g. Condon 1992; Bell et al. 2003; Murphy et al. 2011). This allows us to estimate the level of star formation in high-redshift galaxies, taking advantage of radio observations that are often deeper than FIR surveys with better spatial resolution. The locally observed FRC has also been used to identify samples of radio-loud AGNs and to study their properties (e.g. Donley et al. 2005; Park et al. 2008; Del Moro et al. 2013). Finally, at high redshift, the local FRC has been used to estimate the distance (e.g. Carilli & Yun 1999) or the dust temperature (e.g. Chapman et al. 2005) of luminous starbursts, namely the submillimetre galaxies (SMGs; Smail et al. 1997). As these examples demonstrate, the use of the FRC has become an important tool for extragalactic astrophysics. Upcoming surveys with the Jansky Very Large Array (JVLA) will make its applications even more important.

Although the FRC is characterised well at low redshift, its form and thus its applicability at high redshift still have to be firmly demonstrated. From a theoretical point of view, we expect the FRC to break down at high redshift (i.e. $z \gtrsim 2$–3) because CR electron cooling via inverse Compton (IC) scattering off the cosmic microwave background (CMB; $U_{\rm CMB} \propto (1+z)^4$) photons is supposed to dominate over synchrotron cooling (e.g. Murphy 2009; Lacki & Thompson 2010; Schleicher & Beck 2013). However, the exact redshift and amplitude of this breakdown varies with models and with the assumed properties of high-redshift galaxies. From the observational point of view, the characteristics of the FRC at high redshift have been subject to extensive debate. Some studies have found that the FRC stays unchanged or suffers only minor variations at high redshift (e.g. Appleton et al. 2004; Ibar et al. 2008; Bourne et al. 2011) and others have found significant evolution of the FRC in the bulk of the star-forming galaxy population (e.g. Seymour et al. 2009) or for a subsample of it (e.g. SMGs; Murphy et al. 2009). Sargent et al. (2010) argue that these discrepant measurements could be explained by selection biases due to the improper treatment of flux limits from non-detections amongst radio- and FIR-selected samples. Then, applying a survival analysis to properly treat these non-detections, they conclude that the FRC remains unchanged or with little variations out to $z \sim 1.4$. However, the results of Sargent et al. (2010) were still limited by relatively sparse coverage of the FIR and radio spectral energy distributions (SEDs) of high-redshift galaxies. Noticing these limitations, Ivison et al. (2010a) studied the evolution of the FRC using FIR (250, 350 and 500 μm) observations from BLAST (Devlin et al. 2009) and multi-frequency radio observations (1.4 GHz and 610 MHz). Starting from a mid-infrared-selected sample and accounting for radio non-detections using a stacking analysis, they found an evolution of the FRC with redshift as $\propto(1+z)^{-0.15\pm0.03}$. Repeating a similar analysis using early observations from the *Herschel* Space Observatory, Ivison et al. (2010b) found support for such redshift evolution in the FRC. These findings demand modifications to any high-redshift results that adopted the local FRC. However, because results from Ivison et al. (2010a,b) were based on mid-infrared-selected samples, they might still be affected by some selection biases.

In this paper, we aim to study the FRC across $0 < z < 2.3$, avoiding the biases mentioned above. To obtain a good FIR and radio spectral coverage, we use deep FIR (100, 160, 250, 350 and 500 μm) observations from the *Herschel* Space Observatory (Pilbratt et al. 2010) and deep radio 1.4 GHz VLA and 610 MHz Giant Metre-wave Radio Telescope (GMRT) observations. To minimise selection biases and properly account for radio and FIR non-detections, we use a careful stacking analysis based on the positions of stellar-mass-selected samples of galaxies. These stellar-mass-selected samples are complete for star-forming galaxies down to $10^{10}\,M_\odot$ across $0 < z < 2.3$ and are built from the large wealth of multi-wavelength observations available for the blank extragalactic fields used in our analysis – GOODS-N, GOODS-S, ECDFS and COSMOS.

Besides investigating the evolution of the FRC as a function of redshift, we also aim to study its evolution in the SFR-stellar mass (M_*) plane. Indeed, recent results have shown that the physical properties (e.g. morphology, CO-to-H_2 conversion factor, dust temperature) of star-forming galaxies vary with their positions in the SFR–M_* plane (e.g. Wuyts et al. 2011b; Magnelli et al. 2012b, 2014). In particular, these properties correlate with the distance of a galaxy to the so-called main sequence (MS) of the SFR–M_* plane, i.e. the sequence where the bulk of the star-forming galaxy population resides and which is characterised by $SFR \propto M_*^\gamma$, with $0.5 < \gamma < 1.0$ (Brinchmann et al. 2004; Schiminovich et al. 2007; Noeske et al. 2007; Elbaz et al. 2007; Daddi et al. 2007; Pannella et al. 2009; Dunne et al. 2009; Rodighiero et al. 2010; Oliver et al. 2010; Karim et al. 2011; Mancini et al. 2011; Whitaker et al. 2012). Studying the FRC as a function of the distance of a galaxy from the MS (i.e. $\Delta\log(SSFR)_{\rm MS} = \log[SSFR({\rm galaxy})/SSFR_{\rm MS}(M_*, z)]$) will allow us to estimate if this correlation evolves from normal star-forming galaxies ($\Delta\log(SSFR)_{\rm MS} \sim 0$) to starbursting galaxies ($\Delta\log(SSFR)_{\rm MS} \sim 1$), as suggested by some local observations (e.g. Condon et al. 1991; but see, e.g. Yun et al. 2001).

To study the evolution of the FRC as a function of redshift and as a function of the distance of a galaxy from the MS (i.e. $\Delta\log(SSFR)_{\rm MS}$), we grid the SFR–$M_*$ plane in several redshift ranges and estimate for each SFR–M_*–z bin its infrared luminosity, radio spectral index (i.e. α, where $S_\nu \propto \nu^{-\alpha}$) and radio luminosity using a FIR and radio stacking analysis. Thanks to this methodology, we are able to statistically and accurately constrain the radio spectral index and FRC of all star-forming galaxies with $M_* > 10^{10}\,M_\odot$, $\Delta\log(SSFR)_{\rm MS} > -0.3$ and $0 < z < 2.3$.

Table 1. Main properties of the PEP/GOODS-H/HerMES observations used in this study.

Field		PACS			SPIRE			
		Eff. area arcmin^2	100 μm 3σ^a mJy	160 μm 3σ^a mJy	Eff. area arcmin^2	250 μm 3σ^a mJy	350 μm 3σ^a mJy	500 μm 3σ^a mJy
GOODS-S^b	03^h32^m, $-27°48'$	200 (100)	1.0 (0.6)	2.1 (1.3)	400	7.8	9.5	12.1
ECDFS	03^h32^m, $-27°48'$	900	4.4	8.3	900	7.8	9.1	11.9
GOODS-N	12^h36^m, $+62°14'$	200	1.0	2.1	900	9.2	12	12.1
COSMOS	00^h00^m, $+02°12'$	7344	5.0	10.2	7225	8.1	10.7	15.4

Notes. $^{(a)}$ rms values include confusion noise. $^{(b)}$ Values in parentheses correspond to the PACS ultradeep part of the GOODS-S field, as obtained by combining GOODS-H and PEP observations (Magnelli et al. 2013).

The paper is structured as follows. In Sect. 2 we present the *Herschel*, VLA and GMRT observations used in this study, as well as our stellar-mass-selected sample. Section 3 presents the FIR and radio stacking analysis used to infer the infrared luminosity, radio spectral index and radio luminosity of each of our SFR–M_*–z bins. Evolution of the radio spectral index, $\alpha^{1.4\,\mathrm{GHz}}_{610\,\mathrm{MHz}}$, and of the FRC with $\Delta\log(SSFR)_{\mathrm{MS}}$ and redshift are presented in Sects. 4.1 and 4.2, respectively. Results are discussed in Sect. 5 and summarised in Sect. 6.

Throughout the paper we use a cosmology with $H_0 = 71\,\mathrm{km\,s^{-1}\,Mpc^{-1}}$, $\Omega_\Lambda = 0.73$ and $\Omega_\mathrm{M} = 0.27$.

2. Data

2.1. Herschel observations

To study the FIR properties of galaxies in the SFR–M_* plane, we used deep FIR observations of the COSMOS, GOODS-N, GOODS-S and ECDFS fields provided by the *Herschel* Space observatory. Observations at 100 and 160 μm were obtained by the Photodetector Array Camera and Spectrometer (PACS; Poglitsch et al. 2010) as part of the PACS Evolutionary Probe (PEP[1]; Lutz et al. 2011) guaranteed time key programme and the GOODS-*Herschel* (GOODS-H[2]; Elbaz et al. 2011) open time key programme. Observations at 250, 350 and 500 μm were obtained by the Spectral and Photometric Imaging Receiver (SPIRE Griffin et al. 2010) as part of the *Herschel* Multi-tiered Extragalactic Survey (HerMES[3] Oliver et al. 2012). The PEP, PEP/GOODS-H and HerMES surveys and data reduction methods are described in Lutz et al. (2011), Magnelli et al. (2013, see also Elbaz et al. 2011) and Oliver et al. (2012), respectively. Here we only summarise the information relevant for our study.

Herschel flux densities were derived using a point-spread-function-fitting method, guided by the known position of sources detected in deep 24 μm observations from the Multiband Imaging Photometer (MIPS; Rieke et al. 2004) on board the *Spitzer* Space Observatory. This method provides reliable and highly complete PACS/SPIRE source catalogues (Lutz et al. 2011; Magnelli et al. 2013). We note that the small fraction of *Herschel* sources without a MIPS counterpart and thus missing in our source catalogues (Magdis et al. 2011) will be considered via our stacking analysis which is based on the positions of complete stellar-mass-selected samples (Sect. 3.1). The extraction of PACS sources was accomplished using the method described in Magnelli et al. (2013), while for SPIRE sources it was done using the method described in Roseboom et al. (2010), both using the same 24 μm catalogues. In GOODS-S/N, we used the GOODS 24 μm catalogue, reaching a 3σ limit of 20 μJy (Magnelli et al. 2009, 2011); in the ECDFS, we used the FIDEL 24 μm catalogue, reaching a 3σ limit of 70 μJy (Magnelli et al. 2009); in COSMOS, we used a 24 μm catalogue with a 3σ limit of 45 μJy (Le Floc'h et al. 2009). Reliability, completeness and contamination of our PACS/SPIRE catalogues were tested using Monte Carlo simulations. Table 1 summarises the depths of all these catalogues. Note that SPIRE observations of GOODS-N/S cover much larger effective areas than those from PACS (see Table 1). However, here we restricted our study to regions with both PACS and SPIRE data.

Our MIPS-PACS-SPIRE catalogues were cross-matched with our multi-wavelength catalogues (Sect. 2.4), using their MIPS/IRAC positions and a matching radius of 1″.

2.2. VLA observations

To study the radio properties of our galaxies, we use deep publicly available 1.4 GHz VLA observations. In the COSMOS field, we use observations from the VLA-COSMOS Project[4] (Schinnerer et al. 2004, 2007, 2010). This project has imaged the entire COSMOS field at 1.4 GHz to a mean rms noise of $\sim$10 (15) μJy beam^{-1} across its central 1 (2) deg^2 with a resolution of 1.″5 × 1.″4 (FWHM of the synthesised beam). In the GOODS-N field, we use deep 1.4 GHz VLA observations[5] described in Morrison et al. (2010). This map has a synthesised beam size of 1.″7 × 1.″7 and a mean rms noise of $\sim$3.9 μJy beam^{-1} near its centre, rising to $\sim$8 μJy beam^{-1} at a distance of 15′ from the field centre. Finally, in the GOODS-S and ECDFS fields, we use deep 1.4 GHz VLA observations[6] presented in Miller et al. (2008, 2013). This map has a synthesised beam size of 2.″8 × 1.″6 and an mean rms noise of $\sim$8 μJy beam^{-1}. Table 2 summarises the properties of all these observations.

2.3. GMRT observations

GMRT 610 MHz observations of the GOODS-N and ECDFS fields were obtained in 2009–10 as part of the GOODS-50 project (PI: Ivison). The ECDFS observations were described by Thomson et al. (2014); those of GOODS-N covered a single pointing rather than the six used to cover ECDFS, but in most other respects were identical. The GMRT observations of ECDFS and GOODS-N reach a mean rms noise of $\sim$15 μJy beam^{-1}. The synthesised beam measured 4.″4 × 3.″0 and

[1] http://www.mpe.mpg.de/ir/Research/PEP
[2] http://hedam.oamp.fr/GOODS-Herschel
[3] http://hermes.sussex.ac.uk
[4] http://www.mpia-hd.mpg.de/COSMOS/
[5] http://www.stsci.edu/science/goods/
[6] http://www.astro.umd.edu/~nmiller/VLA_ECDFS.html

Table 2. Main properties of the 1.4 GHz-VLA and 610 MHz-GMRT observations used in this study.

Field	1.4 GHz – VLA		610 MHz – GMRT	
	Eff. area arcmin^2	1σ μJy	Eff. area arcmin^2	1σ μJy
ECDFS & GOODS-S	1156	8	4900	15
GOODS-N	225	3.9–8	400	15
COSMOS[a]	14 400 (3600)	15 (10)	N/A	N/A

Notes. [(a)] Values in parentheses correspond to the deep VLA observations of the centre of the COSMOS field, as obtained by combining data from the VLA-COSMOS Large and Deep project (Schinnerer et al. 2010).

$5\farcs0 \times 4\farcs8$ in the ECDFS and GOODS-N maps, respectively. Table 2 summarises the properties of all these observations.

Note that there are no GMRT observations of the COSMOS field. Therefore, constraints on the radio spectral index of star-forming galaxies (Sect. 4.1) are obtained from a somehow more limited galaxy sample, covering a sky area of ~0.3 deg^2. These limitations could have restrained our ability to constrain the radio spectral index of faint star-forming galaxies. However, we demonstrate in Sect. 3.3 that with our current GMRT observations, we are able to estimate the radio spectral index of galaxies with $M_* > 10^{10}\ M_\odot$, $\Delta\log(SSFR)_{\rm MS} > -0.3$ and $0 < z < 2.3$. These constraints are sufficient for the purpose of our study. In addition, because we do not expect significant cosmic variance, we can apply these constraints obtained on a sky area of ~0.3 deg^2 to our entire galaxy sample.

2.4. Multi-wavelength catalogues

The large wealth of multi-wavelength data used in our study is described in detail in Wuyts et al. (2011a,b; see also Magnelli et al. 2014). Here we only summarise the properties relevant for our study.

In the COSMOS field we used 36 medium and broad-band observations covering the optical to near-infrared SEDs of galaxies (Ilbert et al. 2009; Gabasch et al. 2008). We restricted these catalogues to $i < 25$ and to sources not flagged as problematic in the catalogue of Ilbert et al. (2009). In the GOODS-S field, we used the $K_s < 24.3$ (5σ) FIREWORKS catalogue, providing photometry in 16 bands from U to IRAC wavelengths. In the GOODS-N field, we used the $K_s < 24.3$ (3σ) catalogue created as part of the PEP survey[7], which provides photometry in 16 bands from GALEX to IRAC wavelengths. Finally, in the ECDFS field, we used the $R < 25.3$ (5σ) catalogue described in Cardamone et al. (2010). This multi-wavelength catalogue provides photometry in 18 bands from U to IRAC wavelengths. In the following, ECDFS only corresponds to the outskirts of the original ECDFS region, i.e. when we refer to the ECDFS field, we implicitly exclude the central GOODS-S region.

Spectroscopic redshifts for our galaxies were taken from a combination of various studies (Cohen et al. 2000; Cristiani et al. 2000; Croom et al. 2001; Cimatti et al. 2002, 2008; Wirth et al. 2004; Cowie et al. 2004; Le Fèvre et al. 2004; Szokoly et al. 2004; van der Wel et al. 2004; Mignoli et al. 2005; Vanzella et al. 2006, 2008; Reddy et al. 2006; Barger et al. 2008; Kriek et al. 2008; Lilly et al. 2009; Treister et al. 2009; Balestra et al. 2010). For sources without a spectroscopic redshift, we used photometric redshift computed using EAZY (Brammer et al. 2008) exploiting all the available optical/near-infrared data. The quality of these photometric redshifts was assessed via comparison with spectroscopically confirmed galaxies. The median and median absolute deviation of $\Delta z/(1+z)$ are $(-0.001; 0.013)$ at $z < 1.5$, $(-0.007; 0.066)$ at $z > 1.5$ and $(-0.001; 0.014)$ at $0 < z < 2.3$ (Fig. 1).

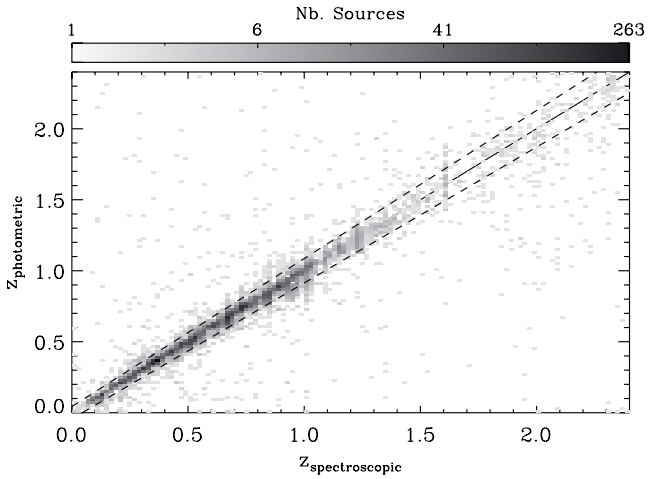

Fig. 1. Comparison between the photometric and spectroscopic redshifts for the 12 132 galaxies with both kinds of redshifts in our multi-wavelength catalogues. Dashed lines represent three times the median absolute deviation found in the redshift range of our study (i.e. $\Delta z/(1+z) = 0.014$ at $0 < z < 2.3$).

2.4.1. Stellar masses

The stellar masses of our galaxies were estimated by fitting all $\lambda_{\rm obs} \leqslant 8\,\mu$m data to Bruzual & Charlot (2003) templates using FAST (Fitting and Assessment of Synthetic Templates; Kriek et al. 2009). The rest-frame template error function of Brammer et al. (2008) was used to down-weight data points with $\lambda_{\rm rest} \geqslant 2\,\mu$m. For those stellar mass estimates we adopted a Chabrier (2003) IMF. Full details on those estimates and their limitations are given in Wuyts et al. (2011a,b).

2.4.2. Star-formation rates

To estimate the SFRs of our galaxies we used the cross-calibrated ladder of SFR indicators established in Wuyts et al. (2011a). This uses the best indicator available for each galaxy and establishes a consistent scale across all of them. For galaxies only detected in the rest-frame UV (i.e. those without a mid- or far-infrared detection), SFRs were estimated from the best fits obtained with FAST. For galaxies with detections both in the rest-frame UV and the mid-/far-infrared, SFRs were estimated by combining the unobscured and re-emitted emission from young stars. This was done following Kennicutt (1998) and adopting a Chabrier (2003) IMF:

$$SFR_{\rm UV+IR}[M_\odot\,{\rm yr}^{-1}] = 1.09\times10^{-10}\,(L_{\rm IR}\,[L_\odot] + 3.3\times L_{2800}\,[L_\odot]), \quad (1)$$

where $L_{2800} \equiv \nu L_\nu(2800\,\text{Å})$ was computed with FAST from the best-fitting SED and the rest-frame infrared luminosity $L_{\rm IR} \equiv L[8-1000\,\mu{\rm m}]$ is derived from the mid-/far-infrared observations. For galaxies with FIR detections, $L_{\rm IR}$ was inferred by fitting their FIR flux densities (i.e. those measured using PACS and

[7] Publicly available at http://www.mpe.mpg.de/ir/Research/PEP

SPIRE) with the SED template library of Dale & Helou (2002, DH), leaving the normalisation of each SED template as a free parameter[8]. The infrared luminosities of galaxies with only a mid-infrared detection were derived by scaling the SED template of MS galaxies (Elbaz et al. 2011) to their 24 μm flux densities. Magnelli et al. (2014) have shown that this specific SED template provides accurate 24 μm-to-$L_{\rm IR}$ conversion factors for such galaxies.

2.4.3. Active galactic nuclei contamination

Active galactic nuclei can affect the observed FRC of star-forming galaxies. Such AGNs must thus be excluded from our sample. To test for the presence of AGNs, we used the deepest available *Chandra* and *XMM-Newton* X-ray observations, identifying AGNs as galaxies with $L_{\rm X}$ [0.5–8.0 keV] $\geq 3 \times 10^{42}$ erg s^{-1} and $L_{\rm X}$ [2.0–10.0 keV] $\geq 3 \times 10^{42}$ erg s^{-1}, respectively (Bauer et al. 2004). In the GOODS-N and -S fields, X-ray observations were taken from the *Chandra* 2-Ms catalogues of Alexander et al. (2003) and Luo et al. (2008), respectively. In the COSMOS field, we used the *XMM-Newton* catalogue of Cappelluti et al. (2009). Finally, for the ECDFS, we used the 250 ks *Chandra* observations, which flank the 2-Ms CDFS observations (Lehmer et al. 2005). All these X-ray-selected AGNs have been removed from our sample. Note that radio-loud AGNs without X-ray detection are excluded in our radio stacking procedure, through use of median stacking (Sect. 3.2).

2.5. Final sample

Our four multi-wavelength catalogues are not homogeneously selected and are not uniform in depth, which naturally translates into different completeness limits in the SFR–M_* plane. These issues have been discussed and studied in Magnelli et al. (2014). They found that in the GOODS-S, GOODS-N and COSMOS fields our multi-wavelength catalogues are complete for star-forming galaxies with $M_* > 10^{10}\,M_\odot$ up to $z \sim 2$. Because the ECDFS multi-wavelength catalogue is based on deeper optical/near-infrared observations than those of the COSMOS field, we conclude that this catalogue also provides us with a complete sample of star-forming galaxies with $M_* > 10^{10}\,M_\odot$ up to $z \sim 2$. In the rest of the paper, we restrict our results and discussion to galaxies with $M_* > 10^{10}\,M_\odot$.

Our final sample contains 8 846, 4 753, 66 070, and 254 749 sources in the GOODS-N, GOODS-S[9], ECDFS and COSMOS fields, respectively. Of these sources, 29%, 26%, 1% and 3% have a spectroscopic redshift, while the rest have photometric redshift estimates. Because we are studying the FRC, the SFR–M_*–z bins that enter our analysis (see Sect. 3) are generally dominated by sources that have individual mid-infrared (and for part of them far-infrared) detections. In GOODS-N, GOODS-S, ECDFS and COSMOS, 19%, 28%, 9% and 12% of the galaxies have mid- or far-infrared detections, respectively. Among those sources, 60%, 45%, 5% and 11% have a spectroscopic redshift.

Figure 2 shows the number density of sources in the SFR–M_* plane. Over a broad range of stellar masses, star-forming galaxies (i.e. excluding massive and passive galaxies situated in the lower right part of the SFR–M_* plane) follow a clear SFR–M_* correlation. This correlation is known as the MS of star formation (Noeske et al. 2007). In the rest of the paper, we parametrise this MS using second-order polynomial functions as derived by Magnelli et al. (2014, see their Table 2). These functions are presented in Fig. 2. Comparisons between this parametrisation and those from the literature are presented and discussed in Magnelli et al. (2014). Briefly, the MS observed in our sample is consistent with the literature at $M_* > 10^{10}\,M_\odot$, i.e. within the stellar mass range of interest for our study.

3. Data analysis

The aim of this paper is to study the evolution of the FRC and radio spectral index with redshift and with respect to the position of galaxies in the SFR–M_* plane. Although we could base this analysis on galaxies individually detected at FIR and/or radio wavelengths, such an approach would be subject to strong limitations, mainly due to complex selection functions (see e.g. Sargent et al. 2010). Instead, we adopted a different approach based on a careful FIR and radio stacking analysis of a stellar-mass-selected sample. This allows us to probe the properties of the FRC and radio spectral index, delving well below the detection limits of current FIR and radio observations. Of course, the use of this stacking analysis has the obvious drawback that one can only study the mean properties of the FRC within the SFR–M_* plane, while outliers are completely missed out. This limitation has to be taken into account while discussing our results. In addition, our stacking analysis has to be performed with great care, especially for the FIR observations where large beam sizes might lead to significant flux biases if the stacked samples are strongly clustered.

3.1. Determination of far-infrared properties through stacking

To estimate the FIR properties (i.e. $L_{\rm FIR}$ and $T_{\rm dust}$) of a given galaxy population, we stacked their *Herschel* observations. The stacking method adopted here is similar to that used in Magnelli et al. (2014). In the following we only summarise the key steps of this method, while for a full description we refer the reader to Magnelli et al. (2014).

For each galaxy population (i.e. for each SFR–M_*–z bin) and for each *Herschel* band, we stacked the residual image (original maps from which we removed all 3σ detections) at the positions of undetected sources (i.e. sources with $S_{Herschel} < 3\sigma$). The stacked stamp of each galaxy was weighted with the inverse of the square of the error map. The flux densities of the final stacked images were measured by fitting with the appropriate PSF. Uncertainties on these flux densities were computed by means of a bootstrap analysis. The mean flux density ($S_{\rm bin}$) of the corresponding galaxy population was then computed by combining the fluxes of undetected and detected sources:

$$S_{\rm bin} = \frac{m \times S_{\rm stack} + \sum_{i=1}^{n} S_i}{n+m}, \quad (2)$$

where $S_{\rm stack}$ is the stacked flux density of the m undetected sources, and S_i is the flux density of the ith detected source (out of a total of n). We note that consistent results are obtained if we repeat the stacking analysis using the original PACS/SPIRE maps and combining all sources in a given SFR–M_*–z bin, regardless of whether they are individually detected or not. We have verified that consistent results are obtained via a median stacking method, rather than the mean stacking described above.

[8] Using the SED template library of Chary & Elbaz (2001) instead of that of DH has no impact on our results.

[9] Although the GOODS-S and -N multi-wavelength catalogues both correspond to $K_{\rm s} < 24.3$, the GOODS-S catalogue contains fewer sources than the GOODS-N catalogue because it includes only sources with >5σ while the GOODS-N multi-wavelength catalogue extends down to a significance of 3σ.

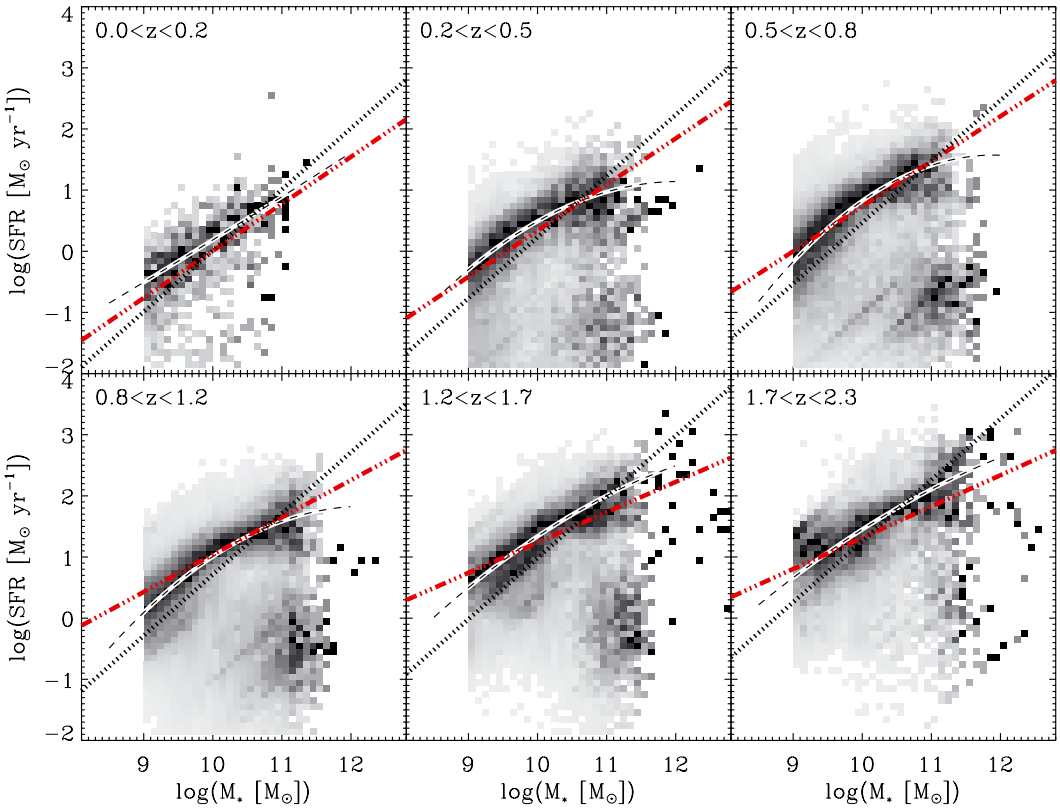

Fig. 2. Number density of sources in the SFR–M_* plane. Shading is independent for each stellar mass bin, i.e. the darkest colour indicates the highest number density of sources in the stellar mass bin and not the highest number density of sources in the entire SFR–M_* plane. Short-dashed lines on a white background show the second-order polynomial functions used here to describe the MS of star formation (Magnelli et al. 2014). Dotted lines represent the MS and its redshift evolution as found in Elbaz et al. (2011). The red triple-dot-dashed lines represent the MS and its redshift evolution as found in Rodighiero et al. (2010).

To verify that the clustering properties of our stacked samples have no significant effect on our stacked FIR flux densities, we used simulations from Magnelli et al. (2014). Briefly, simulated *Herschel* flux densities of all sources in our final sample were estimated using the MS template of Elbaz et al. (2011), given their observed redshifts and SFRs. Simulated *Herschel* maps with real clustering properties were then produced using the observed positions and simulated *Herschel* flux densities of each sources of our fields. Whenever we stacked a given galaxy population on the real *Herschel* images, we also stacked at the same positions the simulated images and thus obtained a simulated stacked flux density ($S^{\rm simu}_{\rm stack}$). Then we compared the $S^{\rm simu}_{\rm stack}$ with the expected mean flux density of this simulated population, i.e. $S^{\rm expected}_{\rm stack}$. If ABS(($S^{\rm simu}_{\rm stack} - S^{\rm expected}_{\rm stack}$)/$S^{\rm expected}_{\rm stack}$) > 0.5, then the real stacked flux densities were identified as being potentially affected by clustering. This 0.5 value was empirically defined as being the threshold above which the effect of clustering would not be captured within the flux uncertainties of our typical $S/N \sim 4$ stacked flux densities. The largest clustering effects are observed at low flux densities and in the SPIRE 500 μm band, as expected. More details on these simulations can be found in Sect. 3.2.2 of Magnelli et al. (2014).

From the mean *Herschel* flux densities of each galaxy population we inferred their rest-frame FIR luminosities (i.e. $L_{\rm FIR}$, where $L_{\rm FIR}$ is the integrated luminosity between 42 μm and 122 μm) and dust temperatures (i.e. $T_{\rm dust}$) by fitting the available FIR photometry using the DH SED template library and a standard χ^2 minimisation method. From the integration of the best-fitting DH SED template, we infer $L_{\rm FIR}$ to within ~0.1 dex, even in cases with only one FIR detection, because *Herschel* observations probe the peak of the FIR emission of galaxies (Elbaz et al. 2011; Nordon et al. 2012). Naturally, we compared these $L_{\rm FIR}$ estimates to the obscured SFR (i.e. $\rm SFR_{IR}$) expected from our ladder of SFR indicators. We reject SFR–M_*–z bins in which these two independent $\rm SFR_{IR}$ estimates are not consistent within 0.3 dex. Such discrepancies are only observed in few SFR–M_*–z bins with stacked FIR flux densities with low significance, $S/N \sim 3$.

From the best-fitting DH SED template we also estimated $T_{\rm dust}$ using the pairing between dust temperature and DH templates established in Magnelli et al. (2014). The reliability of these dust temperature estimates depends on the number of FIR data points available and on whether those data points encompass the peak of the FIR emission. As in Magnelli et al. (2014), we considered as reliable only the dust temperatures inferred from at least three FIR data points encompassing the peak of the FIR emission and with $\chi^2_{\rm reduced} < 3$.

3.2. Determination of the radio properties through stacking

To estimate the radio properties (i.e. $S_{1.4\,\rm GHz}$ and $S_{610\,\rm MHz}$) of a given galaxy population, we stacked their VLA 1.4 GHz and GMRT 610 MHz observations. This stacking analysis is very similar to that employed for the *Herschel* observations. However, the *Herschel* data are very homogeneous among fields, except for the noise level, whereas the radio data differ between fields in properties such as beam shape. Hence, one cannot stack together sources regardless of their position on the sky. Instead,

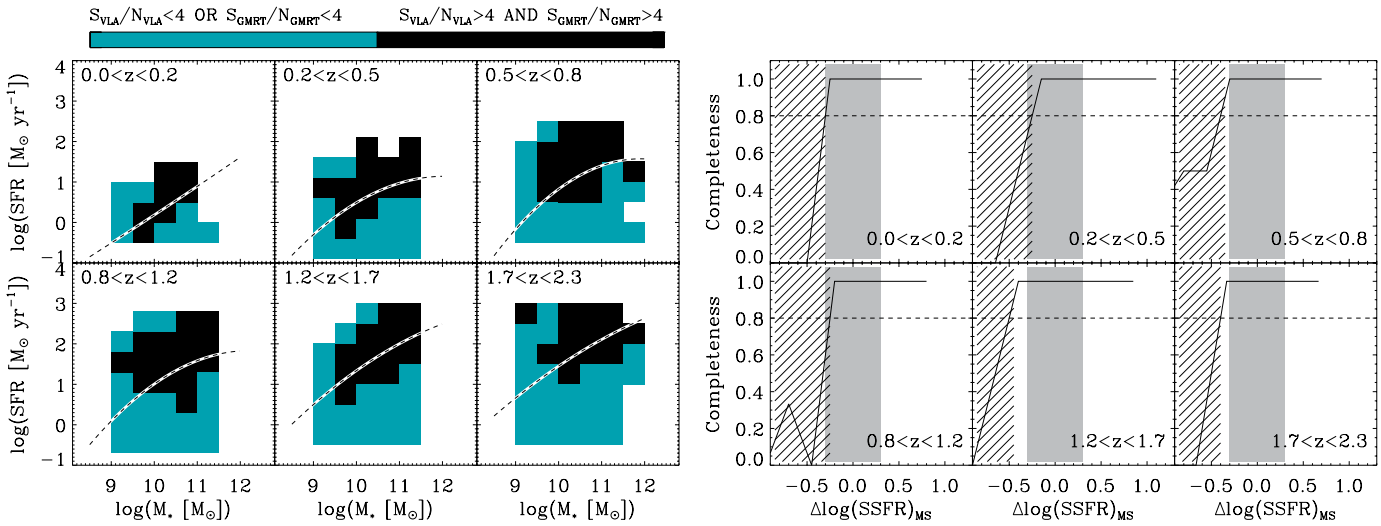

Fig. 3. *Left*: SFR–M_* bins with accurate $\alpha^{1.4\,\mathrm{GHz}}_{610\,\mathrm{MHz}}$ estimates from our stacking analysis. Estimates are considered accurate if $S_{1.4\,\mathrm{GHz}}/N_{1.4\,\mathrm{GHz}} > 4$ (i.e. signal, S, over noise, N, ratio) and $S_{610\,\mathrm{MHz}}/N_{610\,\mathrm{MHz}} > 4$. Short-dashed lines on a white background show the MS of star formation. *Right*: fraction of SFR–M_* bins with $M_* > 10^{10}\,M_\odot$ and with accurate $\alpha^{1.4\,\mathrm{GHz}}_{610\,\mathrm{MHz}}$ estimates as function of their $\Delta\log(SSFR)_{\mathrm{MS}}$. Horizontal dashed lines represent the 80% completeness limits. Hatched areas represent the regions of parameter space affected by incompleteness, i.e. where less than 80% of our SFR–M_* bins have accurate $\alpha^{1.4\,\mathrm{GHz}}_{610\,\mathrm{MHz}}$ estimates. Shaded regions show the location and dispersion of the MS of star formation.

one can stack together sources of the same field, measure their stacked flux densities and associated errors, and finally combine information from different fields using a weighted mean. For a given galaxy population (i.e. a given SFR–M_*–z bin), for each field and each radio band (1.4 GHz and 610 MHz), we thus proceeded as follows. We stacked all sources (regardless of whether they are detected or not) situated in a given field using the original VLA (or GMRT) images. We measured the radio stacked flux density of this galaxy population in this field by fitting their median radio stacked stamp with a 2D Gaussian function. Use of the median avoids the biasing influence of moderately radio-loud AGNs (e.g. Del Moro et al. 2013) that have not yet been removed from the source list via X-ray emission. Because the S/N of our typical radio stacked stamp was poor, in these fits we only left the normalisation of the 2D Gaussian function as a free parameter (i.e. S_{Gaussian}). The position, minor and major axes (i.e. $[a, b]$), and position angle of this 2D Gaussian function were fixed to the values found when fitting the high S/N radio stacked stamp of all galaxies within the current field, redshift bin and with $M_* > 10^{10}\,M_\odot$ and $\Delta\log(SSFR)_{\mathrm{MS}} > -0.3$. The radio stacked flux density of this SFR–M_*–z bin in this field (i.e. S^i_{radio}) was then given by

$$S^i_{\mathrm{radio}} = \frac{S_{\mathrm{Gaussian}} \times a \times b}{a_{\mathrm{norm}} \times b_{\mathrm{norm}}}, \quad (3)$$

where a_{norm} and b_{norm} are the minor and major axes of the radio beam in the original VLA (or GMRT) images. For the VLA observations, where the spatial resolution is relatively high and thus beam smearing by astrometric uncertainties in the stacked samples can be significant, S_{radio} were ∼1.9 times higher than S_{Gaussian}. Despite astrometric uncertainties, galaxy sizes marginally resolved at the ∼1.5″ resolution of the VLA observations might also explain part of the difference between S_{radio} and S_{Gaussian}. The appropriate uncertainty on this radio flux density was obtained from a bootstrap analysis. Finally, we combined the radio stacked flux densities of a given SFR–M_*–z bin from different fields (i.e. GOODS-N, GOODS-S, ECDFS and COSMOS) using a weighted mean.

From their stacked 1.4 GHz flux densities, we derived the rest-frame 1.4 GHz luminosity (i.e. $L_{1.4\,\mathrm{GHz}}$) for our SFR–M_*–z bins. For that, we k-corrected their stacked 1.4 GHz flux density assuming a radio spectral index of $\alpha = 0.8$ (e.g. Condon 1992; Ibar et al. 2009, 2010). This value is perfectly in line with the radio spectral index observed here (i.e. $\alpha^{1.4\,\mathrm{GHz}}_{610\,\mathrm{MHz}}$) over a broad range of redshift and $\Delta\log(SSFR)_{\mathrm{MS}}$ (see Sect. 4.1).

3.3. The SFR-M_*-z parameter space

Before looking at the evolution of the FRC and radio spectral index in the SFR–M_*–z parameter space, we need to ensure that our ability to make accurate q_{FIR} and $\alpha^{1.4\,\mathrm{GHz}}_{610\,\mathrm{MHz}}$ measurements does not introduce significant incompleteness in any particular regions of the SFR–M_* plane. The left panels of Figs. 3 and 4 present the regions of the SFR–M_*–z parameter space with accurate $\alpha^{1.4\,\mathrm{GHz}}_{610\,\mathrm{MHz}}$ and q_{FIR} estimates from our stacking analysis, respectively. The sampling of the SFR–M_* plane is made with larger SFR–M_* bins for $\alpha^{1.4\,\mathrm{GHz}}_{610\,\mathrm{MHz}}$ than for q_{FIR}. This is due to the fact that the GMRT observations covered a sky area of only 0.3 deg^2 (Sect. 2.3). This limited dataset forces us to enlarge the size of our SFR–M_* bins in order to increase the number of stacked sources per bin and thus improve the noise in our stacked stamps ($\sigma_{\mathrm{stack}} \propto \sqrt{N}$). Our $\alpha^{1.4\,\mathrm{GHz}}_{610\,\mathrm{MHz}}$ estimates are considered as accurate only if $S_{1.4\,\mathrm{GHz}}/N_{1.4\,\mathrm{GHz}} > 4$ and $S_{610\,\mathrm{MHz}}/N_{610\,\mathrm{MHz}} > 4$. Our q_{FIR} estimates are considered as accurate only if $S_{1.4\,\mathrm{GHz}}/N_{1.4\,\mathrm{GHz}} > 3$ and L_{FIR} is reliable (see Sect. 3.1). In each of our redshift bins, our stacking analysis allows us to obtain accurate $\alpha^{1.4\,\mathrm{GHz}}_{610\,\mathrm{MHz}}$ and q_{FIR} estimates for almost all MS and above-MS galaxies with $M_* > 10^{10}\,M_\odot$.

The right panels of Figs. 3 and 4 illustrate our ability to study the variations of $\alpha^{1.4\,\mathrm{GHz}}_{610\,\mathrm{MHz}}$ and q_{FIR} for galaxies with $M_* > 10^{10}\,M_\odot$, respectively. In these figures we show the fraction of SFR–M_* bins with reliable $\alpha^{1.4\,\mathrm{GHz}}_{610\,\mathrm{MHz}}$ or q_{FIR} estimates as a function of their $\Delta\log(SSFR)_{\mathrm{MS}}$. In the rest of the paper, we consider that $\alpha^{1.4\,\mathrm{GHz}}_{610\,\mathrm{MHz}}$ or q_{FIR} in a given $\Delta\log(SSFR)_{\mathrm{MS}}$ bin is fully constrained only if the completeness in this bin is ≳80%. In each

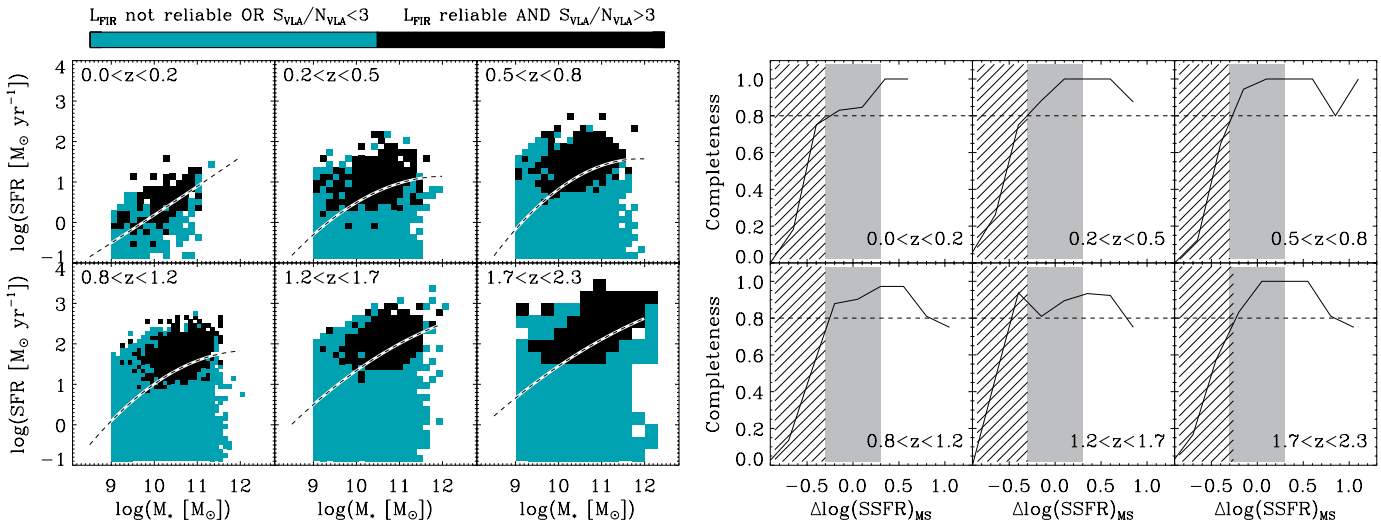

Fig. 4. *Left*: SFR–M_* bins with accurate $q_{\rm FIR}$ estimates from our stacking analysis. Estimates are considered accurate if $S_{1.4\,\rm GHz}/N_{1.4\,\rm GHz} > 3$ (i.e. signal, S, over noise, N, ratio) and $L_{\rm FIR}$ is reliable (see Sect. 3.1). Short-dashed lines on a white background show the MS of star formation. *Right*: fraction of SFR–M_* bins with $M_* > 10^{10}\,M_\odot$ and with accurate $q_{\rm FIR}$ estimates as function of their $\Delta\log(SSFR)_{\rm MS}$. Horizontal dashed lines represent the 80% completeness limits. Hatched areas represent the regions of parameter space affected by incompleteness. Shaded regions show the location and dispersion of the MS of star formation.

redshift bin, our stacking analysis allows us to fully constrain $\alpha^{1.4\,\rm GHz}_{610\,\rm MHz}$ and $q_{\rm FIR}$ in galaxies with $\Delta\log(SSFR)_{\rm MS} > -0.3$.

From this analysis, we conclude that our stacking analysis provides us with a complete view on the evolution of $\alpha^{1.4\,\rm GHz}_{610\,\rm MHz}$ and $q_{\rm FIR}$ up to $z \sim 2$ in star-forming galaxies with $M_* > 10^{10}\,M_\odot$ and $\Delta\log(SSFR)_{\rm MS} > -0.3$.

4. Results

4.1. The radio spectral index, $\alpha^{1.4\ GHz}_{610\ MHz}$

The radio spectral index of each SFR–M_*–z bin was inferred using their VLA and GMRT stacked flux densities, i.e. $S_{1.4\,\rm GHz}$ and $S_{610\,\rm MHz}$, respectively. Assuming that the radio spectrum follows a power law form, $S_\nu \propto \nu^{-\alpha}$, the radio spectral index is given by,

$$\alpha^{1.4\,\rm GHz}_{610\,\rm MHz} = \frac{\log(S_{610\,\rm MHz}/S_{1.4\,\rm GHz})}{\log(1400/610)}. \quad (4)$$

$S_{1.4\,\rm GHz}$ and $S_{610\,\rm MHz}$ are *observed* flux densities. Therefore, at different redshift, $\alpha^{1.4\,\rm GHz}_{610\,\rm MHz}$ correspond to radio spectral indices at different rest-frame frequencies. This has to be taken into account when interpreting our results (see Sect. 5.1.2). In the following, we discuss only accurate $\alpha^{1.4\,\rm GHz}_{610\,\rm MHz}$ estimates. We remind the reader that constraints on the radio spectral index of star-forming galaxies are obtained from a somewhat limited galaxy sample, covering a sky area of ~0.3 deg^2, as GMRT observations of the COSMOS fields are not available.

The Fig. 5 presents the evolution of $\alpha^{1.4\,\rm GHz}_{610\,\rm MHz}$ as a function of $\Delta\log(SSFR)_{\rm MS}$ up to $z \sim 2$. We find no strong correlation between $\alpha^{1.4\,\rm GHz}_{610\,\rm MHz}$ and $\Delta\log(SSFR)_{\rm MS}$ in any redshift bin (i.e. $|\rho_{\rm s}| \lesssim 0.6$) and the null hypothesis of uncorrelated data cannot be rejected with high significance (i.e. Sig. >5%). In addition, the median $\alpha^{1.4\,\rm GHz}_{610\,\rm MHz}$ does not deviate significantly from the canonical value, 0.8 (e.g. Condon 1992), in any of our redshift bins. From these findings we conclude that most star-forming galaxies with $M_* > 10^{10}\,M_\odot$ and across $0 < z < 2.3$ have on average a radio spectral index consistent with 0.8. However, due to the relatively low number of data points and to the large dispersion on $\alpha^{1.4\,\rm GHz}_{610\,\rm MHz}$, we cannot confidently rule out the presence of a negative, but weak, $\alpha^{1.4\,\rm GHz}_{610\,\rm MHz} - \Delta\log(SSFR)_{\rm MS}$ correlation ($\rho_{\rm s} < 0$). Such a trend would echo (but not match) the results of Condon et al. (1991, see also Clemens et al. 2008) who found that the most extreme local starbursts have flatter radio spectra (i.e. ~0.5) than local normal star-forming galaxies (i.e. ~0.8). Condon et al. (1991) and Clemens et al. (2008) attribute these flat radio spectra to free-free absorption in dense nuclear starbursts.

The Fig. 6 shows that our results agree well with the range of radio spectral index observed in a large sample of sub-mJy radio galaxies (Ibar et al. 2009) and in a population of $z \sim 2$ SMGs (Ibar et al. 2010, see also Thomson et al. 2014). These agreements are re-assuring because results from Ibar et al. (2009, 2010) and Thomson et al. (2014) were based on galaxies individually detected in the VLA and GMRT images.

Our results are also in line with those of Bourne et al. (2011) and Ivison et al. (2010a). Both studies are based on a stacking analysis, but Ivison et al. (2010a) applied it to a sample of 24 μm-selected (i.e. SFR-selected) galaxies while Bourne et al. (2011) applied it to a stellar-mass-selected galaxy sample (including both star-forming and quiescent galaxies). The consistencies observed between studies with different selection functions reinforce our conclusion that $\alpha^{1.4\,\rm GHz}_{610\,\rm MHz}$ does not significantly evolve across $0 < z < 2.3$. We note that results from our study and those from Ivison et al. (2010a) and Bourne et al. (2011) are, however, not strictly independent since they are based on the same VLA and similar GMRT observations of ECDFS. Nevertheless, we believe that the consistencies found here are noteworthy because those studies differ in many other aspects: our stacking analysis includes observations from the GOODS-N field; our GMRT observations of ECDFS are deeper; our stellar-mass-selected sample is built using different optical-to-near-IR multi-wavelength catalogues, applying different methods to infer photometric redshifts and stellar masses.

The absence of significant evolution in $\alpha^{1.4\,\rm GHz}_{610\,\rm MHz}$ with z and $\Delta\log(SSFR)_{\rm MS}$ is an important result for our forthcoming study of the FRC. Indeed, to k-correct our stacked 1.4 GHz flux densities into rest-frame 1.4 GHz radio luminosities, we

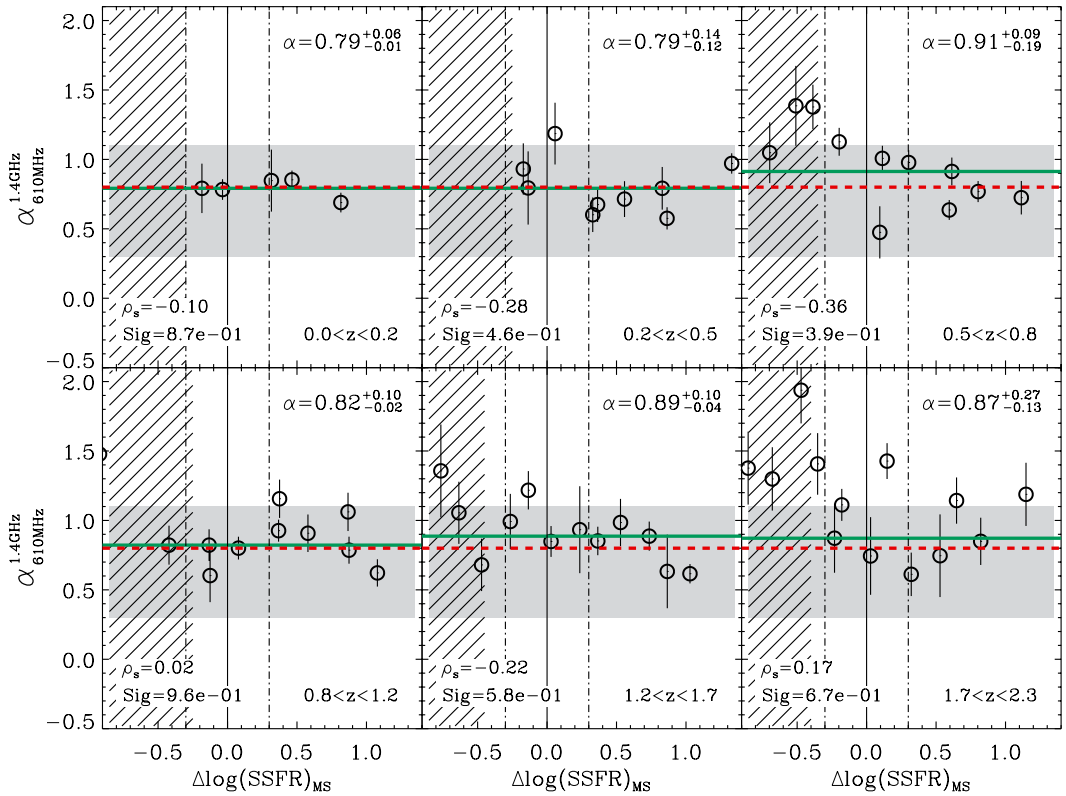

Fig. 5. Radio spectral index (i.e. $\alpha^{1.4\,\mathrm{GHz}}_{610\,\mathrm{MHz}}$) of galaxies as a function of $\Delta\log(SSFR)_{\mathrm{MS}}$, as derived from our stacking analysis. Hatched areas represent the regions of parameter space affected by incompleteness (see text and Fig. 3). In each panel, we give the median value (see also the green lines), the Spearman rank correlation (ρ_s) and the null hypothesis probability (Sig.) derived from data points in the region of parameter space not affected by incompleteness. Red dashed lines correspond to the *canonical* radio spectral index of 0.8 observed in local star-forming galaxies (Condon 1992) and high-redshift SMGs (Ibar et al. 2010). Shaded regions show the range of $\alpha^{1.4\,\mathrm{GHz}}_{610\,\mathrm{MHz}}$ values (i.e. 0.7 ± 0.4) observed by Ibar et al. (2009) in a population of sub-mJy radio galaxies. Vertical solid and dot-dashed lines show the localisation and width of the MS of star formation. In the range of redshift and $\Delta\log(SSFR)_{\mathrm{MS}}$ probed here, $\alpha^{1.4\,\mathrm{GHz}}_{610\,\mathrm{MHz}}$ does not significantly deviate from its canonical value, 0.8.

assumed that the radio spectral index of *all* galaxies across $0 < z < 2.3$ was equal to 0.8 (see Sect. 3.2). Significant deviations from this canonical value would have introduced artificial evolution of the FRC in the SFR–M_*–z parameter space ($\Delta q_{\mathrm{FIR}} = -\Delta\alpha \times \log(1+z)$).

The physical implications of the absence of significant evolution of $\alpha^{1.4\,\mathrm{GHz}}_{610\,\mathrm{MHz}}$ with z and $\Delta\log(SSFR)_{\mathrm{MS}}$ are discussed in Sect. 5.

4.2. The FIR/radio correlation

Using the rest-frame FIR and 1.4 GHz luminosities estimated from our stacking analysis, we study the evolution of the FRC in the SFR–M_*–z parameter space. For that, we use the parametrisation of the FRC given in Helou et al. (1988; see also Yun et al. 2001),

$$q_{\mathrm{FIR}} = \log\left(\frac{L_{\mathrm{FIR}}[\mathrm{W}]}{3.75\times10^{12}}\right) - \log\left(L_{1.4\,\mathrm{GHz}}\left[\mathrm{W\,Hz^{-1}}\right]\right), \quad (5)$$

where L_{FIR} is the integrated FIR luminosity from rest-frame 42 to 122 μm and $L_{1.4\,\mathrm{GHz}}$ is the rest-frame 1.4 GHz radio luminosity density. Radio k-corrections are inferred assuming $S_\nu \propto \nu^{-\alpha}$ and the canonical radio spectral index of $\alpha = 0.8$ (see Sect. 4.1; Condon 1992). In the recent literature, alternative parametrisations of the FRC have been proposed. In particular, some studies have used the infrared luminosity from rest-frame 8 to 1000 μm (L_{IR}) instead of L_{FIR} (e.g. Ivison et al. 2010a,b; Sargent et al. 2010; Bourne et al. 2011). Such different definitions have no significant impact because there is a tight relation between L_{FIR} and L_{IR} of star-forming galaxies. Over all our SFR–M_*–z bins, we indeed found $L_{\mathrm{IR}} = 1.91^{+0.10}_{-0.05} \times L_{\mathrm{FIR}}$. Thus, to compare q_{FIR} with q_{IR}, we simply corrected these estimates following $q_{\mathrm{FIR}} = q_{\mathrm{IR}} - \log(1.91)$.

The Fig. 7 shows the evolution of q_{FIR} in the SFR–M_* plane in different redshift bins. In this figure, we do not identify any significant and systematic evolution of q_{FIR} in the SFR–M_* plane. In contrast, we notice a clear and systematic decrease in q_{FIR} with redshift.

In Fig. 8 we investigate the existence of more subtle evolution of q_{FIR} within the SFR–M_* plane by plotting the variation of q_{FIR} as a function of $\Delta\log(SSFR)_{\mathrm{MS}}$. In all our redshift bins, there is a weak ($0.1 \lesssim |\rho_s| \lesssim 0.4$) correlation between q_{FIR} and $\Delta\log(SSFR)_{\mathrm{MS}}$, though the null hypothesis of uncorrelated data can only be rejected with high significance (i.e. Sig. < 5%) in two of these redshift bins (i.e. $0.5 < z < 0.8$ and $0.8 < z < 1.2$). In addition, at high $\Delta\log(SSFR)_{\mathrm{MS}}$, the dispersion on q_{FIR} seems to increase.

To study further the statistical significance of a weak q_{FIR} – $\Delta\log(SSFR)_{\mathrm{MS}}$ correlation, we fit this relation with a constant and with a linear function using a Monte-Carlo approach taking into account errors both on q_{FIR} and $\Delta\log(SSFR)_{\mathrm{MS}}$. Data points used in these fits are restricted to those situated in regions of parameter space not affected by incompleteness. For each of our 1000 Monte-Carlo realisations, we adopt new values of q_{FIR} and $\Delta\log(SSFR)_{\mathrm{MS}}$ selected into a Gaussian distribution centred on their original values and with a dispersion

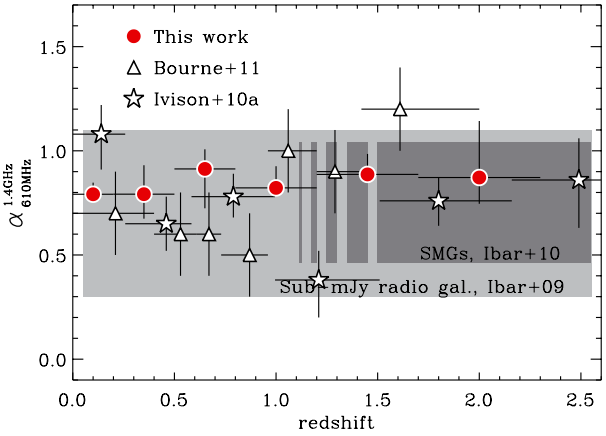

Fig. 6. Evolution of the radio spectral index, $\alpha_{610\,\mathrm{MHz}}^{1.4\,\mathrm{GHz}}$, with redshift, as inferred from our stacking analysis. Red circles and error bars correspond to the median and interquartile range observed in our study in regions of the parameter space not affected by incompleteness (see values and green lines reported in Fig. 5). Stars show results from Ivison et al. (2010a), while triangles show results from Bourne et al. (2011). Both studies are based on a stacking analysis, but Ivison et al. (2010a) applied it to a sample of 24 μm-selected galaxies while Bourne et al. (2011) applied it to a stellar-mass-selected galaxy sample. The light grey region shows the range of $\alpha_{610\,\mathrm{MHz}}^{1.4\,\mathrm{GHz}}$ values (i.e. 0.7 ± 0.4) observed by Ibar et al. (2009) in a population of sub-mJy radio galaxies. The dark grey region presents the range of $\alpha_{610\,\mathrm{MHz}}^{1.4\,\mathrm{GHz}}$ values (i.e. 0.75 ± 0.29) observed in a population of SMGs at $z \sim 2$ (Ibar et al. 2010). Note that the ranges of values observed in Ibar et al. (2009, 2010) correspond to the intrinsic dispersion observed in these galaxy populations and not to measurement errors on the mean radio spectral indices.

given by their measurement errors. To ensure that our fits are not dominated by few data points, for each Monte-Carlo realisation we resample the observed dataset, keeping its original size but randomly selecting its data points with replacement. We then fit each Monte-Carlo realisation with a constant and with a linear function. Finally, we study the mean value and dispersion of each fitting parameter across our 1000 Monte-Carlo realisations.

In all but the $0.5 < z < 0.8$ redshift bin, the constant model has reduced χ^2 values lower than those of the linear model. In addition, in these redshift bins, the linear model has slopes (i.e. $\Delta[q_{\mathrm{FIR}}]/\Delta[\Delta\log(SSFR)_{\mathrm{MS}}]$) consistent, within 1σ, with zero. This suggests that there is no significant $q_{\mathrm{FIR}} - \Delta\log(SSFR)_{\mathrm{MS}}$ correlation in these redshift bins. In contrast, at $0.5 < z < 0.8$, the linear model is statistically slightly better than the constant model (i.e. $\chi^2_{\mathrm{red}}[\mathrm{linear}] = 7.0$ and $\chi^2_{\mathrm{red}}[\mathrm{cst}] = 7.5$) and its slope is different to zero at the $\sim 3\sigma$ level (i.e. 0.22 ± 0.07). This suggests a positive but weak $q_{\mathrm{FIR}} - \Delta\log(SSFR)_{\mathrm{MS}}$ correlation[10] at $0.5 < z < 0.8$. We note that it is also in this redshift bin that our measurement errors on q_{FIR} are the lowest. This could explain why an intrinsically weak $q_{\mathrm{FIR}} - \Delta\log(SSFR)_{\mathrm{MS}}$ correlation can only be statistically significant at $0.5 < z < 0.8$.

This Monte-Carlo approach demonstrates that the existence of a $q_{\mathrm{FIR}} - \Delta\log(SSFR)_{\mathrm{MS}}$ correlation is yet difficult to assess from our dataset. If there exists a $q_{\mathrm{FIR}} - \Delta\log(SSFR)_{\mathrm{MS}}$ correlation, it is intrinsically weak. Unfortunately, our observations are not good enough to firmly reveal or rule out such weak correlation in all our redshift bins. Thus, we conservatively conclude that there is no significant $q_{\mathrm{FIR}} - \Delta\log(SSFR)_{\mathrm{MS}}$ correlation across $0 < z < 2.3$, though the presence of a weak, positive trend, as observed in one of our redshift bin ($0.5 < z < 0.8$), cannot be firmly ruled out using our dataset. Note that debates on the existence of a weak $q_{\mathrm{FIR}} - \Delta\log(SSFR)_{\mathrm{MS}}$ correlation also prevail in the local Universe. Condon et al. (1991) found that the most extreme local starbursts (i.e. $\Delta\log(SSFR)_{\mathrm{MS}} \sim 1$) have higher q_{FIR} and larger dispersions of q_{FIR} than normal star-forming galaxies (i.e. $\Delta\log(SSFR)_{\mathrm{MS}} \sim 0$). In contrast, Helou et al. (1985) and Yun et al. (2001) do not report any statistically significant increase in q_{FIR} in extreme starbursts, though they also found a larger dispersion in q_{FIR} for this population.

While q_{FIR} does not significantly evolve with $\Delta\log(SSFR)_{\mathrm{MS}}$, its median value clearly decreases smoothly with redshift. To study this trend we plot in Fig. 9 the redshift evolution of the median and interquartile range of q_{FIR}, observed in regions of parameter space not affected by incompleteness. We find a statistically significant (Sig. <1%) redshift evolution of q_{FIR}. This evolution can be parametrised using,

$$q_{\mathrm{FIR}}(z) = (2.35 \pm 0.08) \times (1+z)^{-0.12\pm0.04} \quad (6)$$

where the $z = 0$ value of this function agrees perfectly with local observations, i.e. $q_{\mathrm{FIR}}(z \sim 0) \approx 2.34 \pm 0.26$ (Yun et al. 2001). If we parametrise this redshift evolution separately for normal ($\Delta\log(SSFR)_{\mathrm{MS}} < 0.75$) and starbursting galaxies ($\Delta\log(\mathrm{SSFR})_{\mathrm{MS}} > 0.75$)[11], we end up with similar solutions, i.e. $q_{\mathrm{FIR}}(z) = (2.42 \pm 0.08) \times (1+z)^{-0.16\pm0.05}$ and $q_{\mathrm{FIR}}(z) = (2.44 \pm 0.09) \times (1+z)^{-0.13\pm0.09}$, respectively. We note that while the evolution of q_{FIR} with redshift is statistically significant, it is moderate. Indeed, at $z \sim 2$, the median value of q_{FIR} is still within the 1σ dispersion of local observations (Yun et al. 2001).

This redshift evolution of q_{FIR} could not be artificially introduced by a redshift evolution of the radio spectral index. Indeed, to create such evolution, the radio spectral index would need to change from 0.8 to 0.2 between $z = 0$ and $z = 2$, respectively ($\Delta q_{\mathrm{FIR}} = -\Delta\alpha \times \log(1+z)$). Such extreme redshift evolution of the radio spectral index is not observed in our sample (see Fig. 6 and Sect. 4.1).

In Fig. 9 we compare our findings with those from the literature. In the past decade many papers have discussed this topic. Therefore, instead of presenting an exhaustive comparison, we compare our findings with the three papers which are, we believe, the most relevant, i.e. those based on relatively complete and well understood samples and/or valuable FIR/radio datasets. Firstly, we compare our results with those of Bourne et al. (2011). In that paper, the authors overcame the selection biases of radio- and/or infrared-selected samples by using a stellar-mass-selected sample in the ECDFS. The infrared and radio properties of their galaxies at a given stellar mass and redshift were then inferred by stacking *Spitzer* (24, 70 and 160 μm) and VLA observations. This approach is thus very similar to that employed here. Secondly, we compare our results with those of Sargent et al. (2010). This paper used a large sample of infrared- and radio-selected galaxies in the COSMOS field. To overcome selection biases, Sargent et al. (2010) applied a careful survival analysis to the *Spitzer* (24 and 70 μm) and VLA catalogues. Finally, we compare our results with those of Ivison et al. (2010b). In this paper, the authors used *Herschel* observations of the GOODS-N field to constrain the redshift evolution of q_{FIR} on a relative small sample of L_{IR}-matched galaxies.

Results from the literature are in broad agreement with our conclusions. Data from Bourne et al. (2011) exhibit a consistent $q_{\mathrm{FIR}} - z$ correlation, though with a slight overall offset of their

[10] This positive correlation will not be erased but rather enhanced where a weak negative $\alpha_{610\,\mathrm{MHz}}^{1.4\,\mathrm{GHz}} - \Delta\log(SSFR)_{\mathrm{MS}}$ correlation exists (see Sect. 4.1).

[11] This definition of starbursts is consistent with that of Rodighiero et al. (2011).

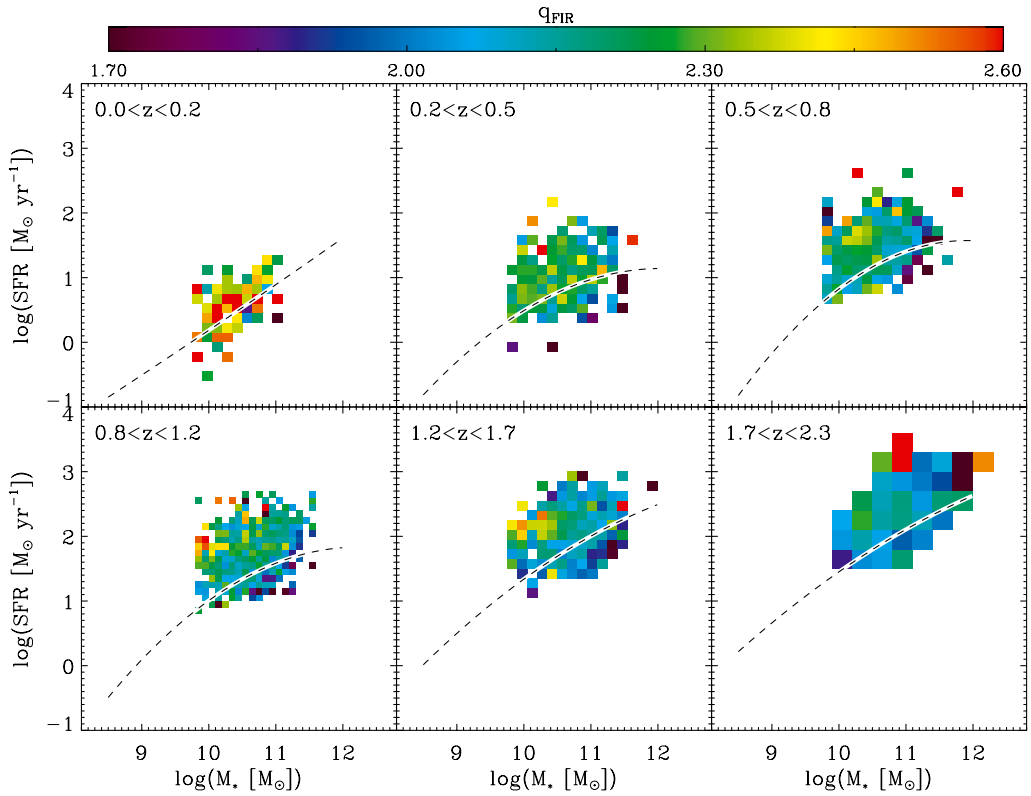

Fig. 7. Evolution of the mean $L_{\rm FIR}$ – to – $L_{1.4\,\rm GHz}$ ratio, i.e. $q_{\rm FIR}$ (see Eq. (5)), of galaxies in the SFR–M_* plane, as found using our stacking analysis. Short-dashed lines on a white background show the MS of star formation.

$q_{\rm FIR}$ values ($\Delta q_{\rm FIR} \sim 0.15$). Bourne et al. (2011) also noticed that their $q_{\rm FIR}$ values were systematically higher than that expected from local observations. They attributed this offset to difference in the assumptions made to infer $L_{\rm IR}$ from *Spitzer* observations. Most likely, the overall offset observed here between their and our measurements has the same origin.

Results from Ivison et al. (2010b) also exhibit a clear decrease in $q_{\rm FIR}$ with redshift. However, here as well there exists some disagreement with respect to our measurements: the decrease in $q_{\rm FIR}$ starts at $z > 0.7$, and at $0.7 < z < 1.4$, their measurements of $q_{\rm FIR}$ are significantly higher. These discrepancies could not be explained by difference in the assumptions made to derive $L_{\rm FIR}$, because both studies used FIR observations from *Herschel*. Instead, these discrepancies might be explained by cosmic variance and/or by some differences in our sample selection. For example, at $z \sim 0.5$, the measurement of Ivison et al. (2010b) relied on only 16 galaxies and they argued that it might need to be discounted. In addition, the sample of Ivison et al. (2010b) is $L_{\rm IR}$-selected and not SFR–M_*-selected, and still includes X-ray sources.

The results of Sargent et al. (2010) are perfectly in line with our findings. They found a clear decrease in $q_{\rm FIR}$ with redshift, and the amplitude and normalisation of their $q_{\rm FIR} - z$ correlation is consistent with our measurements.

From all these comparisons, we conclude that results from the literature are also broadly consistent with a decrease in $q_{\rm FIR}$ with redshift. Note, however, that these studies have mostly chosen to favour a non-evolving scenario for the FRC. This moderate redshift evolution of $q_{\rm FIR}$, which remains within its local 1σ dispersion even at $z \sim 2$, was not deemed sufficiently significant in most of these studies, which relied on relatively small samples with sparse FIR and radio spectral coverage. Our sample is sufficiently large and well controlled (i.e. complete for star-forming galaxies with $M_* > 10^{10}\,M_\odot$) with excellent FIR and radio spectral coverage to conclude that $q_{\rm FIR}$ evolves with redshift as $q_{\rm FIR} \propto (1+z)^{-0.12\pm0.04}$. Possible physical explanations and implications of this redshift evolution are discussed in Sect. 5.

In Fig. 10, we consider the reality of a correlation between $q_{\rm FIR}$ and $T_{\rm dust}$. In all our redshift bins, there is a weak, positive $q_{\rm FIR} - T_{\rm dust}$ correlation; in four bins we can reject the null hypothesis of uncorrelated data with high significance (Sig. <5%). However, using our Monte-Carlo approach to fit this relation, we find that only at $0.5 < z < 0.8$ the linear model has better reduced χ^2 values than the constant model and has a slope different than zero at the $\sim 3\sigma$ level (i.e. $\Delta[q_{\rm FIR}]/\Delta[T_{\rm dust}] = 0.023 \pm 0.008$). For the other redshift bins, the linear and constant models are statistically undistinguishable and the slopes of the linear model are consistent, within 1σ, with zero. Thus, we conclude that the existence of a $q_{\rm FIR} - T_{\rm dust}$ correlation is statistically meaningful in only one of our redshift bin. Such $q_{\rm FIR} - T_{\rm dust}$ correlation could be related to the weak, positive $q_{\rm FIR} - \Delta\log(SSFR)_{\rm MS}$ correlation observed in the same redshift bin, because $T_{\rm dust}$ is known to be positively correlated with $\Delta\log(SSFR)_{\rm MS}$ (Magnelli et al. 2014). Note, however, that our estimates of $T_{\rm dust}$ might be affected/contaminated by AGN emission, complicating the interpretation on the existence of a $q_{\rm FIR} - T_{\rm dust}$ correlation.

5. Discussion

5.1. Evolution of the radio spectra

Our results indicate that the radio spectral index, $\alpha^{1.4\,\rm GHz}_{610\,\rm MHz}$, does not significantly evolve with redshift, does not correlate significantly with $\Delta\log(SSFR)_{\rm MS}$ and is consistent everywhere with its canonical value of 0.8 (see Figs. 5 and 6). Those results

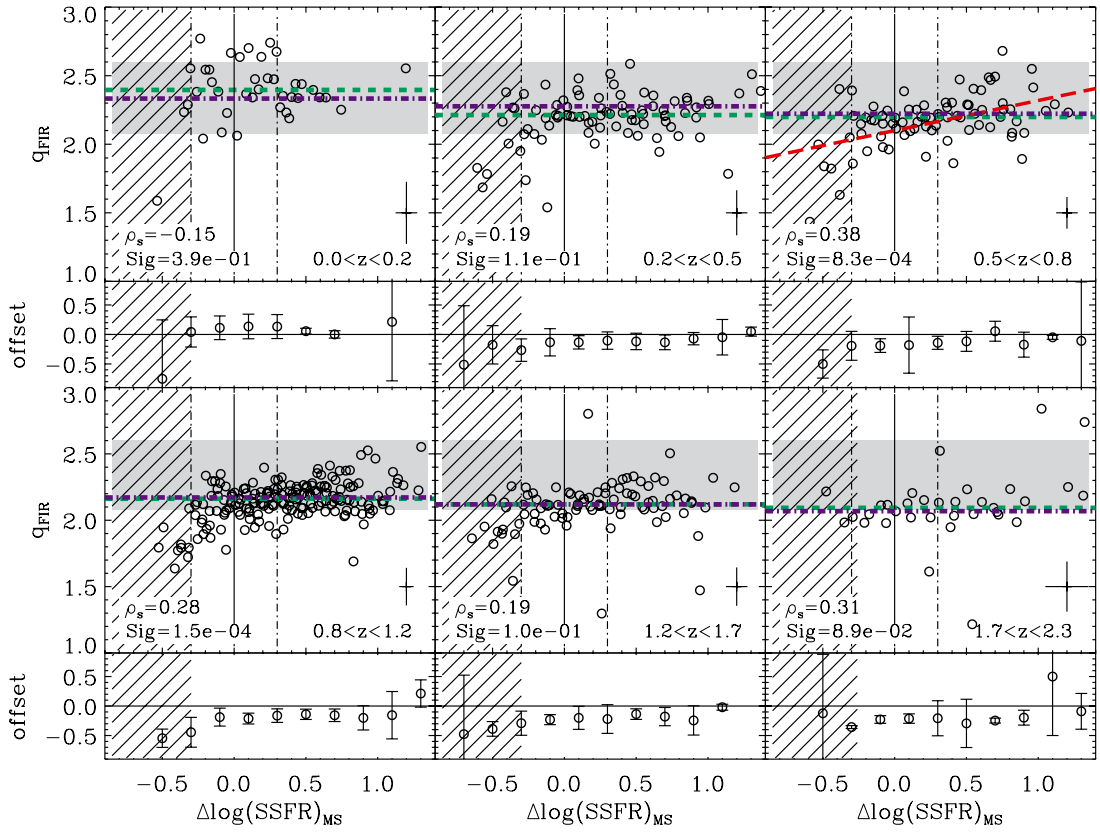

Fig. 8. Mean L_{FIR} – to – $L_{1.4\,GHz}$ ratio (q_{FIR}) of galaxies as a function of $\Delta\log(SSFR)_{MS}$, as derived from our stacking analysis. Hatched areas represent the regions of parameter space affected by incompleteness (see text and Fig. 4), while the light grey region shows the value of q_{FIR} observed by Yun et al. (2001) in a large sample of local star-forming galaxies, $q_{FIR}(z \sim 0) = 2.34 \pm 0.26$. In each panel, we show the median value (green dashed line), give the Spearman rank correlation (ρ_s) and the null hypothesis probability (Sig.) derived from data points in the region of parameter space not affected by incompleteness. Blue dot-dashed lines represent a redshift evolution of $q_{FIR} = 2.35 \times (1+z)^{-0.12}$. In the lower right part of each panel, we give the median uncertainty on our q_{FIR} estimates. Vertical solid and dot-dashed lines show the localisation and the width of the MS of star formation. In the redshift bin with a statistically significant correlation (Sig. <5% and χ^2_{red}[linear] < χ^2_{red}[cst], see text), we plot (red long-dashed line) a linear fit, $q_{FIR} = (0.22 \pm 0.07) \times \Delta\log(SSFR)_{MS} + (2.10 \pm 0.05)$. The lower panel of each redshift bin shows the offset between the median q_{FIR} of our data and the local value of $q_{FIR}(z = 0) \approx 2.34$, in bins of 0.2 dex.

are valid for all star-forming galaxies with $M_* > 10^{10}\,M_\odot$, $\Delta\log(SSFR)_{MS} > -0.3$ and $0 < z < 2.3$.

5.1.1. AGN contamination?

Some may find the absence of significant redshift evolution in α surprising, perhaps anticipating the rapid increase in the AGN population at $z > 1$ (e.g. Hasinger et al. 2005; Wall et al. 2005) and their influence on the observed radio spectral index of their host galaxies. At low redshift and therefore low rest-frame frequencies, AGNs can exhibit flat radio spectra ($\alpha < 0.5$; e.g. Murphy 2013) while at higher redshift and thus higher rest-frame frequencies they can exhibit steep radio spectra ($\alpha > 1.0$; e.g. Huynh et al. 2007). With the increasing number of AGNs at $z > 1$, one might then expect variations in the radio spectral index inferred from our statistical sample. However, since our goal is to explore the properties of star-forming galaxies, and anticipating the possible impact of AGNs, we excluded the brightest X-ray AGNs from our sample and used a *median* radio stacking method. This should have minimised any AGN contamination. Interestingly, if we stack our bright X-ray AGNs, we find radio spectra indices in the range [0.7−1.0][12]. This suggests that the radio spectral index of the bulk of the X-rays AGN population is dominated by emission from their host galaxies. Note, however, that the AGN contribution to the radio emission of a galaxy could also have a radio spectral index of ∼0.75. Indeed, while the radio emission of the compact core of AGNs is supposed to have a flat spectrum at low frequencies and a steep spectrum at high frequencies, their extended radio emission associated with lobes is supposed to have a power-law spectrum with $\alpha \sim 0.75$ (Jackson & Wall 1999).

5.1.2. Nature of the radio spectra

Our VLA and GMRT observations probe different rest-frame radio frequencies at different redshifts. Consequently, even if all star-forming galaxies have the same intrinsic radio spectra, one could still expect to observe redshift evolution of $\alpha^{1.4\,GHz}_{610\,MHz}$ in the presence of a curved spectrum. Such redshift evolution of $\alpha^{1.4\,GHz}_{610\,MHz}$ is not observed in our sample, suggesting that in the range of rest-frame frequencies probed here, 610 MHz < ν_{rest} < 4.2 GHz, the radio spectra are well described by a power-law function with $S_\nu \propto \nu^{-0.8}$. The radio spectra of high-redshift

[12] Precisely, we found $\alpha^{1.4\,GHz}_{610\,MHz} = 1.0 \pm 0.1$, 0.7 ± 0.1, 0.8 ± 0.1 and 0.7 ± 0.1 for X-ray AGNs at $0.5 < z < 0.8$, $0.8 < z < 1.2$, $1.2 < z < 1.7$ and $1.7 < z < 2.3$, respectively. Unfortunately, the numbers of X-ray AGNs at $z < 0.5$ is not large enough to obtain a meaningful estimate of $\alpha^{1.4\,GHz}_{610\,MHz}$ using our sample.

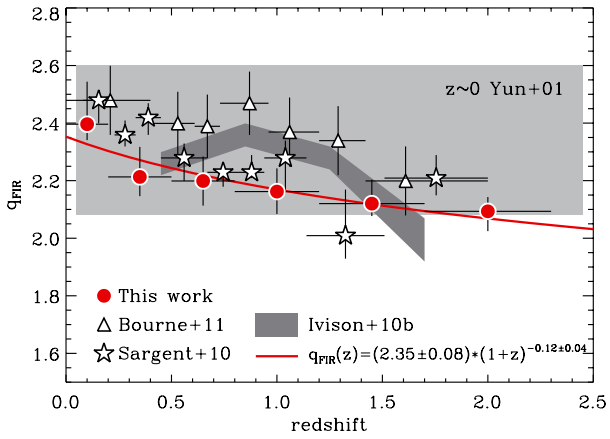

Fig. 9. Evolution of the L_{FIR} – to – $L_{1.4\,GHz}$ ratio, q_{FIR}, with redshift, as inferred from our stacking analysis. Red circles and error bars correspond to the median and interquartile range observed in our study in regions of the parameter space not affected by incompleteness (green dashed lines in Fig. 8). The red line corresponds to a redshift-dependent fit to our data points, $q_{FIR}(z) = 2.35 \times (1 + z)^{-0.12}$. The light grey region shows the value of q_{FIR} observed by Yun et al. (2001) in a large sample of local star-forming galaxies, $q_{FIR}(z \sim 0) = 2.34 \pm 0.26$. This *local* measurement is displayed over the entire range of redshift to highlight any possible redshift evolution of q_{FIR}. The dark grey region presents results from Ivison et al. (2010b) using *Herschel* observations on a L_{IR}-matched sample. Empty triangles show results from Bourne et al. (2011), as inferred using a stacking analysis on a stellar-mass-selected sample of galaxies. Stars present results obtained by Sargent et al. (2010) using a FIR/radio-selected sample of star-forming galaxies and applying a survival analysis to properly treat flux limits from non-detections.

star-forming galaxies seem to be dominated by non-thermal optically thin synchrotron emission with the same properties as that observed in the local Universe; thermal free-free emission with relatively flat radio spectra (i.e. $\alpha \sim 0.1$) does not dominate their rest-GHz radio spectra. Unfortunately, these conclusions might be compromised if the constant $\alpha^{1.4\,GHz}_{610\,MHz}$ value is caused by a conspiracy, involving a curved radio spectra and some intrinsic evolution with redshift.

In the local Universe, starbursts/ULIRGs have significantly flatter radio spectra ($\alpha \sim 0.5$) than normal star-forming galaxies ($\alpha \sim 0.8$; Condon et al. 1991; Clemens et al. 2008). While our sample might exhibit some flattening of the radio spectral index when moving from the MS regime ($\Delta\log(SSFR)_{MS} \sim 0$) to the starburst regime ($\Delta\log(SSFR)_{MS} \sim 1$), these $\alpha^{1.4\,GHz}_{610\,MHz}$ – $\Delta\log(SSFR)_{MS}$ correlations are weak and statistically insignificant (Sig. >5%). The observation in high-redshift starbursts of steeper radio spectra than in the local Universe echoes results for samples of SMGs, which also have $\alpha \sim 0.8$ (Ibar et al. 2010; Thomson et al. 2014). Indeed, luminous SMGs are situated well above the MS (Magnelli et al. 2012a), are believed to be strong starbursts and to be the high-redshift counterparts of local ULIRGs. The fact that high-redshift starbursts have steeper radio spectra suggests that they may not have the same ISM conditions as their local counterparts, as already hinted by numerous other studies looking at their size (e.g. Tacconi et al. 2006; Biggs & Ivison 2008; Farrah et al. 2008) and physical properties (e.g. Ivison et al. 2010c; Farrah et al. 2008). Alternatively, it could indicate that the flatter radio spectra of local ULIRGs are due to low-frequency free-free absorption, as advocated by Condon et al. (1991), a less relevant effect at the higher rest-frame frequencies probed at high redshift, though at $z \sim 2$ our data are not probing above ~4 GHz.

5.1.3. Expectations from theory

Using a single-zone model of CR injection, cooling and escape, Lacki et al. (2010, hereafter L10) and Lacki & Thompson (2010, hereafter LT10) explore the radio spectra of normal and starburst galaxies and their evolution with redshift. At $z \sim 0$, their model predicts a relatively flat radio spectrum at rest-GHz frequencies for compact starbursts ($\alpha \sim 0.5$) and a steeper spectrum for normal star-forming galaxies ($\alpha \sim 0.8$), though this difference decreases at higher rest-frame frequencies ($\gg$10 GHz) where both asymptote to $\alpha \sim 1.1$. The flatter radio spectrum of starbursts is attributed to more efficient Bremsstrahlung and ionisation cooling of CR electrons and positrons in their dense ISM. Thus, the L10 model predicts the observed flatter radio spectra of local ULIRGs but contradicts the hypothesis of Condon et al. (1991) about its origin via free-free absorption.

Our observations do not reveal a significant decrease in the radio spectral index as we move from normal star-forming galaxies ($\Delta\log(SSFR)_{MS} \sim 0$) to starbursts ($\Delta\log(SSFR)_{MS} \sim 1$). Instead, high-redshift starbursts seem to have roughly the same radio spectral index as normal star-forming galaxies. As already mentioned, this result was hinted by the observation of steeper radio spectra and more extended star-forming regions in high-redshift SMGs than in local ULIRGs. Therefore, LT10 suggested that high-redshift SMGs have larger CR scale heights ($h \sim 1$ kpc), consistent with that observed in local normal star-forming galaxies. This large CR scale height leads to less efficient Bremsstrahlung and ionisation cooling of CRs and thus steeper radio spectra. Our results suggest that the bulk of the high-redshift starburst population, and not only SMGs, may have large CR scale heights, labelled puffy starbursts in LT10.

LT10 also predict evolution of the radio spectral index of galaxies with redshift. Combining intrinsic evolution of the radio spectra with k-correction considerations, they find that $\alpha^{1.4\,GHz}_{610\,MHz}$ of normal star-forming galaxies and their puffy starbursts should evolve from ~0.8 to ~1.0 between $z \sim 0$ and $z \sim 2$. The evolution for compact starbursts is predicted to be weaker, $\alpha^{1.4\,GHz}_{610\,MHz}$ increasing from ~0.5 to ~0.6 between $z \sim 0$ and $z \sim 2$. In both cases the steepening of the radio spectra is attributed to the increase with redshift in IC losses from the CMB. In our analysis we do not find any significant increase in $\alpha^{1.4\,GHz}_{610\,MHz}$ with redshift. However, our large measurements errors on α ($\sigma^{measurements}_{\alpha} \sim 0.1$–$0.2$) and the existence of large intrinsic dispersion as revealed by studies of individually detected high-redshift galaxies ($\sigma^{intrinsic}_{\alpha} \sim 0.3$; Ibar et al. 2009, 2010) prevents us from ruling out the possibility that high-redshift star-forming galaxies follow the expectations of LT10 for normal star-forming galaxies and puffy starbursts. Further insight into any subtle evolution of α with redshift (as well as with $\Delta\log(SSFR)_{MS}$) will require deeper multi-frequency radio observations.

5.2. Evolution of the FIR/radio correlation

Our results indicate that the FRC evolves with redshift as $q_{FIR}(z) = (2.35 \pm 0.08) \times (1 + z)^{-0.12\pm0.04}$ (see Fig. 9). They also indicate that the FRC does not significantly evolve with $\Delta\log(SSFR)_{MS}$, though the presence of a weak positive trend, as observed in one of our redshift bin (i.e. $\Delta[q_{FIR}]/\Delta[\Delta\log(SSFR)_{MS}] = 0.22 \pm 0.07$ at $0.5 < z < 0.8$), cannot be firmly ruled out using our dataset (see Fig. 8). These results are valid for all star-forming galaxies with $M_* > 10^{10}\,M_\odot$, $\Delta\log(SSFR)_{MS} > -0.3$ and $0 < z < 2.3$.

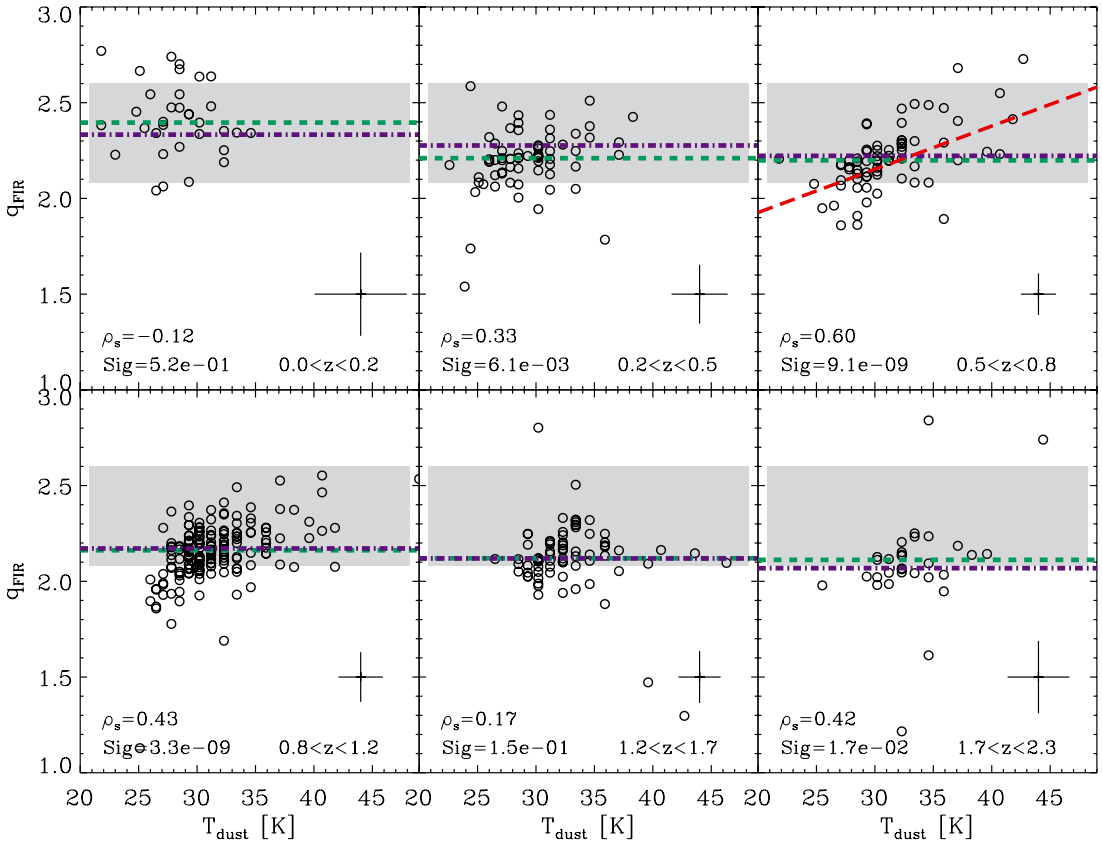

Fig. 10. Mean $L_{\rm FIR}$ – to – $L_{1.4\,\rm GHz}$ ratio ($q_{\rm FIR}$) of galaxies as a function of dust temperature, as derived from our stacking analysis. In each panel, we give the Spearman rank correlation ($\rho_{\rm s}$), the null hypothesis probability (Sig.), and show the median uncertainties on our $q_{\rm FIR}$ and $T_{\rm dust}$ estimates. In the redshift bin with a statistically significant (Sig. <5% and $\chi^2_{\rm red}$[linear] < $\chi^2_{\rm red}$[cst]) correlation, we plot (red long-dashed lines) a linear fit, $q_{\rm FIR} = (0.023 \pm 0.008) \times T_{\rm dust} + (1.47 \pm 0.32)$. The rest of the lines and shaded region are the same as in Fig. 8.

5.2.1. AGN contamination?

The presence of a large population of AGNs in our sample at $z > 1$ might be a concern for our $q_{\rm FIR}$ estimates. Anticipating this problem, we have removed X-ray AGNs from our sample and used a *median* radio stacking analysis to statistically exclude the relatively small population of radio-loud AGNs. However, these precautions will minimise but not completely eliminate contamination by AGNs. To further reduce this potential contamination, we repeat our stacking analysis removing from our sample AGNs selected by the IRAC colour-colour criteria of Lacy et al. (2007)[13]. This selection should exclude of our analysis obscured AGNs missed in X-ray observations (Lacy et al. 2007; Stern et al. 2005; Donley et al. 2012). We found 11 865 IRAC AGNs in our sample, of which 4347 have individual mid-infrared detections. This corresponds to ∼4% of our final sample and ∼12% of our final sample with individual mid-infrared detections. Excluding IRAC AGNs does not change qualitatively and quantitatively our results: $q_{\rm FIR}$ smoothly decreases by ∼0.3 across $0 < z < 2.3$ and there is no significant $q_{\rm FIR} - \Delta\log(SSFR)_{\rm MS}$ correlation. We conclude that the decrease in $q_{\rm FIR}$ is most likely not driven by AGN contamination. Note that this absence of significant contamination from AGNs echoes results from Sargent et al. (2010; see also Bonzini et al., in prep.). Indeed, using individually detected FIR and radio sources, Sargent et al. (2010) found that AGNs (X-ray selected and optically selected) and star-forming galaxies follow the same FRC (in terms of normalisation and dispersion) out to at least $z \sim 1.4$.

5.2.2. Expectations from theory

Theory predicts that the FRC is driven by star-formation activity in galaxies. The UV emission of young, massive ($\gtrsim 8\,M_\odot$) stars is absorbed by dust and re-emitted in the FIR. This creates a linear correlation between SFR and $L_{\rm IR}$, if galaxies are optically thick at UV wavelengths. After few Myrs, young massive stars explode into SNe, accelerating CRs into the general magnetic field of galaxies and resulting in diffuse synchrotron emission. Thus, when averaged over the star-formation episode (neglecting the short lag between the UV emission and explosion of the first massive young stars), we expect a clear link between SFR, FIR and radio synchrotron emission from star-forming galaxies. This constitutes the essence of the calorimeter theory first proposed in Völk (1989). In this theory, galaxies are both UV and electron calorimeters, i.e. *all* UV radiation from young stars is re-emitted by dust in the FIR and *all* CR electrons are converted within the galaxies into an observable form, mainly via synchrotron CR cooling.

The calorimeter theory has however been questioned, especially in light of the remarkably tight FRC over three orders of magnitude in luminosity. L10 proposed that – on top of calorimetry – a number of additional physical processes conspire to yield such a tight FRC, covering dwarf galaxies and

[13] Donley et al. (2012) have proposed more restrictive IRAC AGN colour−colour criteria to decrease the contamination by star-forming galaxies. However, because the completeness in term of AGN selection of these more restrictive IRAC criteria might be lower, we decided to use the original Lacy et al. (2007) definition.

ULIRGs. At low SFR surface density ($\Sigma_{\rm SFR}$[14]), the UV calorimeter assumption fails: galaxies are not optically thick and some UV photons escape without being re-emitted in the FIR (e.g. Buat et al. 2005). At the same time, the CR electrons calorimeter assumption also fails. CR electrons escape without radiating their energy in the radio, placing the galaxies back onto the FRC. At high $\Sigma_{\rm SFR}$, CR cooling via Bremsstrahlung, ionisation and IC processes become more important because of higher gas densities. CR cooling via synchrotron competes with these processes, decreasing the radio synchrotron emission of compact starbursts. However, because of the higher gas densities, compact starbursts become CR proton calorimeters. CR protons convert their energy via inelastic scattering into gamma rays, neutrinos and secondary protons and electrons. These secondary protons and electrons undergo synchrotron cooling, placing compact starbursts back onto the FRC. From this, L10 conclude that calorimetry combines with several conspiracies operating in different density regimes to produce a relatively constant (variation <0.3) FRC across the range $0.001\,M_\odot\,{\rm kpc}^{-2}\,{\rm yr}^{-1} < \Sigma_{\rm SFR} < 1000\,M_\odot\,{\rm kpc}^{-2}\,{\rm yr}^{-1}$.

Other theories have been proposed to explain the FRC. For example Schleicher & Beck (2013, hereafter S13; see also Niklas & Beck 1997) explained the FRC by relating star formation and magnetic field strength via turbulent magnetic field amplification, the so-called small-scale dynamo effect. This model explains the FRC of galaxies both globally and on kiloparsec scales. Contrary to the findings of L10, this model predicts that the FRC should evolve with $\Sigma_{\rm SFR}$ as $q_{\rm FIR} = -0.3\times\log(\Sigma_{\rm SFR})+C_1$.

- *Is the FRC expected to evolve with* $\Delta\log(SSFR)_{\rm MS}$*?*
We can relate $\Delta\log(SSFR)_{\rm MS}$ with $\Sigma_{\rm SFR}$ using estimates presented in Wuyts et al. (2011b) and based on almost the same galaxy sample used here (see Sect. 2.4). Wuyts et al. (2011b) found that $\Sigma_{\rm SFR}$ increases linearly with $\Delta\log(SSFR)_{\rm MS}$. At $z \sim 0.1$, MS galaxies ($\Delta\log(SSFR)_{\rm MS} \sim 0$) have $\Sigma_{\rm SFR} \sim 0.02\,M_\odot\,{\rm kpc}^{-2}\,{\rm yr}^{-1}$ while starbursts ($\Delta\log({\rm SSFR})_{\rm MS} \sim 1$) have $\Sigma_{\rm SFR} \sim 0.2\,M_\odot\,{\rm kpc}^{-2}\,{\rm yr}^{-1}$. At $z \sim 2.0$, MS galaxies have $\Sigma_{\rm SFR} \sim 1\,M_\odot\,{\rm kpc}^{-2}\,{\rm yr}^{-1}$ while starbursts have $\Sigma_{\rm SFR} \sim 10\,M_\odot\,{\rm kpc}^{-2}\,{\rm yr}^{-1}$ (for more details, see Fig. 4 of Wuyts et al. 2011b). Thus, in a given redshift bin, our analysis probes at least one order of magnitude in $\Sigma_{\rm SFR}$. Across this range, the model of L10 expects no significant evolution[15] of $q_{\rm FIR}$, while the model of S13 expects $q_{\rm FIR}$ to decrease by 0.3. Here, we find that, if it exists, a $q_{\rm FIR} - \Delta\log(SSFR)_{\rm MS}$ correlation is necessary weak and rather positive ($\Delta[q_{\rm FIR}]/\Delta[\Delta\log(SSFR)_{\rm MS}] = 0.22 \pm 0.07$). This result disfavours the model of S13.
- *Is the FRC expected to evolve with redshift?*
LT10 and S13 also study the evolution of the FRC with redshift. At high redshift the main concern is that other CR cooling processes might start to dominate over synchrotron. In particular, IC cooling from the CMB might become dominant at high redshift ($U_{\rm CMB} \propto (1+z)^4$), leading to a significant increase in $q_{\rm FIR}$ (see also Murphy 2009). However, both studies concluded that the FRC should hold with no dramatic break-down (i.e. $q_{\rm FIR}(z) - q_{\rm FIR}(z=0) \gtrsim 0.5$) out to relatively high redshift: up to $z \sim 2$ (8) for galaxies with $\Sigma \sim 1\,M_\odot\,{\rm kpc}^{-2}\,{\rm yr}^{-1}$ and up to $z \sim 3$ (15) for galaxies with $\Sigma \sim 10\,M_\odot\,{\rm kpc}^{-2}\,{\rm yr}^{-1}$ in S13 (LT10). Because at $z \sim 2$ our galaxies have $\Sigma_{\rm SFR} > 1\,M_\odot\,{\rm kpc}^{-2}\,{\rm yr}^{-1}$, none of these models expect a dramatic increase in $q_{\rm FIR}$ for our sample. These expectations are in line with our results.

Apart from this potential break-down of the FRC due to IC cooling from the CMB, LT10 also study the possibility of more subtle variations of the FRC with redshift. Because SMGs exhibited low $q_{\rm FIR}$ values ($q_{\rm FIR} \sim 2.0$; Murphy et al. 2009) and steep radio spectra ($\alpha \sim 0.8$; Ibar et al. 2010), LT10 postulate that high-redshift SMGs have larger CR scale heights than their local counterparts ($h \sim 1$ kpc instead of $h \sim 0.1$ kpc). Then, assuming that the magnetic field strength varies with $\Sigma_{\rm gas}$ and not $\rho_{\rm gas}$, they find that such large CR scale heights decrease the CR losses via Bremsstrahlung and ionisation processes, increasing the synchrotron emission and decreasing $q_{\rm FIR}$ by ~0.3. LT10 argue that such puffy starbursts are also supported by kinematic observations of SMGs, citing Tacconi et al. (2006). From this, LT10 predict two different evolution of $q_{\rm FIR}$ across the range $0.001\,M_\odot\,{\rm kpc}^{-2}\,{\rm yr}^{-1} < \Sigma_{\rm SFR} < 1000\,M_\odot\,{\rm kpc}^{-2}\,{\rm yr}^{-1}$. In their normal-to-compact starburst track, $q_{\rm FIR}$ remains constant as a function of $\Sigma_{\rm SFR}$, while in their normal-to-puffy starburst track $q_{\rm FIR}$ significantly evolves with $\Sigma_{\rm SFR}$. In this latter, normal star-forming galaxies and puffy starbursts have the same CR scale height and $q_{\rm FIR}$ smoothly decreases by 0.3 from $\Sigma_{\rm SFR} = 0.001\,M_\odot\,{\rm kpc}^{-2}\,{\rm yr}^{-1}$ to $\Sigma_{\rm SFR} = 1\,M_\odot\,{\rm kpc}^{-2}\,{\rm yr}^{-1}$ and then $q_{\rm FIR} \sim 2$ at $\Sigma_{\rm SFR} \gtrsim 1\,M_\odot\,{\rm kpc}^{-2}\,{\rm yr}^{-1}$. Therefore, while LT10 do not formally predict a particular redshift evolution of $q_{\rm FIR}$, they expect that if the CR scale height of star-forming galaxies evolve with redshifts, $q_{\rm FIR}$ should evolve accordingly. At $z \sim 2$, all our galaxies have $\Sigma_{\rm SFR} > 1\,M_\odot\,{\rm kpc}^{-2}\,{\rm yr}^{-1}$ and their $q_{\rm FIR}$ have decreased by 0.3. These observations suggest that most high-redshift star-forming galaxies may have CR scale heights of ~1 kpc, not only SMGs. This is in qualitative agreement with the finding that many high-redshift MS star-forming galaxies are clumpy disks with larger disk velocity dispersions (and hence scale heights) than local spirals (e.g. Förster Schreiber et al. 2009; Newman et al. 2013).

S13 also predict some subtle variations of $q_{\rm FIR}$ with redshift following,

$$q_{\rm FIR} = -0.3\log(\Sigma_{\rm SFR}) - \frac{4\beta}{6}\log(1+z) + C_2, \quad (7)$$

where β parametrises the evolution of the typical ISM density of galaxies with redshift, $\rho = \rho_0\,(1+z)^\beta$. For MS galaxies, $\Sigma_{\rm SFR}$ increases by 1.7 dex from $z \sim 0$ to $z \sim 2$. Assuming that their CR scale heights stay the same across this redshift range ($h \sim 1$ kpc) and that $\Sigma_{\rm SFR} = \Sigma_{\rm gas}^N \sim (h\,\rho)^N$ with $N \sim 1$–2 from the Schmidt-Kennicutt relation, one would infer that $\rho_{z\sim2}^{\rm MS} = \rho_{z=0}^{\rm MS}\,(1+z)^{\beta_{\rm MS}}$ with $\beta_{\rm MS} \sim 1.8$–3.6. Using the model of S13, we therefore predict that $q_{\rm FIR}$ for MS galaxies should decrease by -1.0 (-1.6) between $z \sim 0$ and $z \sim 2$ for $N = 2$ (1). Such large evolution of $q_{\rm FIR}$ is not supported by our observations. Similarly, one can predict the evolution of $q_{\rm FIR}$ for starbursts galaxies ($\Delta\log(SSFR)_{\rm MS} \gtrsim 0.75$). Their $\Sigma_{\rm SFR}$ also increase by 1.7 dex from $z \sim 0$ to $z \sim 2$. Assuming that their CR scale heights evolve from $h \sim 0.1$ kpc to $h \sim 1$ kpc from $z \sim 0$ to $z \sim 2$, we predict – using the model of S13 – a decrease in $q_{\rm FIR}$ by -0.4 (-1.0) for $N = 2$ (1) across this redshift range[16]. Again, such large evolution of $q_{\rm FIR}$ is not supported by our observations.

[14] Or equivalently low $\Sigma_{\rm gas}$, according to the Schmidt-Kennicutt-relation, $\Sigma_{\rm SFR} \propto \Sigma_{\rm gas}^N$ with $N = 1$–2.

[15] This is true even if high-redshift galaxies follow the normal-to-puffy starburst track of LT10. Indeed, at $z \sim 2$, our galaxies have $\Sigma_{\rm SFR} > 1\,M_\odot\,{\rm kpc}^{-2}\,{\rm yr}^{-1}$, a $\Sigma_{\rm SFR}$ regime where LT10 expect constant $q_{\rm FIR}$.

[16] Assuming that the CR scale height of starbursts is 0.1 kpc across $0 < z < 2.3$, we infer similar evolution of $q_{\rm FIR}$ than for MS galaxies, i.e. $-1.0 < \Delta q_{\rm FIR} < -1.6$.

- *Is the FRC expected to evolve with redshift in the context of the MS of star formation?*
  There is strong observational evidence that the physical conditions reigning in the star-forming regions of high-redshift MS galaxies are similar to those of normal local star-forming galaxies, though high-redshift MS galaxies have larger $\Sigma_{\rm SFR}$ (Wuyts et al. 2011b; Elbaz et al. 2011; Nordon et al. 2012; Magnelli et al. 2012b, 2014). Thus, MS galaxies should follow the normal-to-puffy starburst track of LT10 across $0 < z < 2.3$, with its constant CR scale height of ∼1 kpc. This would translate into a smooth decrease in $q_{\rm FIR}$ by 0.3 at $z \sim 2$ as their $\Sigma_{\rm SFR}$ varies from $\Sigma_{\rm SFR} \sim 0.02\,M_\odot\,{\rm kpc}^{-2}\,{\rm yr}^{-1}$ to $\Sigma_{\rm SFR} \sim 1\,M_\odot\,{\rm kpc}^{-2}\,{\rm yr}^{-1}$ across this redshift range. Such predictions are supported by our observations.
  In contrast, the decrease in $q_{\rm FIR}$ with redshift for far-above MS galaxies (those with $\Delta\log(SSFR)_{\rm MS} \gtrsim 0.75$, see Sect. 4.2) is more surprising. Indeed, at high redshift, far-above MS galaxies are thought to be starbursts with similar FIR properties to local ULIRG (e.g. Elbaz et al. 2011; Magnelli et al. 2012b, 2014). Consequently, one could expect these galaxies to follow the compact starburst predictions of LT10 across $0 < z < 2.3$, characterised by a constant value of $q_{\rm FIR}$ over a large range of $\Sigma_{\rm SFR}$. Instead, their $q_{\rm FIR}$ seems to decrease by ∼0.3 at $z \sim 2$, suggesting that most high-redshift starbursts (and not only SMGs) have larger CR scale heights (puffy starbursts) than their local counterparts (compact starbursts). Consequently, while high-redshift starbursts seems to share some physical properties with local ULIRGs (FIR SEDs; CO-to-H_2 conversion factors), other properties seem to be significantly different (size of their star-forming regions and CR scale heights). Note, however, that there is a larger dispersion of $q_{\rm FIR}$ at high $\Delta\log(SSFR)_{\rm MS}$ values and that the $q_{\rm FIR} - z$ correlation is statistically less significant for far-above MS galaxies than for MS galaxies ($q_{\rm FIR}[z, \text{far-above MS}] \propto (1+z)^{-0.13\pm0.09}$ and $q_{\rm FIR}[z, \text{MS}] \propto (1+z)^{-0.16\pm0.05}$). This supports a more complex scenario in which a non-negligible number of high-redshift starbursts are associated with compact starbursts rather than with puffy starbursts.

5.2.3. Implications of the evolution with redshifts of the FRC

Our results have important implications for previous and future studies relying on the FRC. For example, SFRs of high-redshift galaxies determined via radio observations will be lower than expected from the local FRC. However, while the evolution of $q_{\rm FIR}$ with redshift is statistically significant, it is modest and still lies within its local 1σ dispersion at $z \sim 2$. Thus, corrections of SFRs motivated by our findings should still be within the uncertainties inferred using the local 1σ dispersion of the FRC.

Our results have also important implications for our understanding of the contribution of star-forming galaxies to the radio extragalactic background. In particular, an extragalactic 3.3 GHz radio background of $\nu I_\nu \approx 5.9 \times 10^{-4}\,{\rm nW\,m^{-2}\,sr^{-1}}$ has been detected with ARCADE2 (Fixsen et al. 2011; Seiffert et al. 2011). The sources of this cosmic radio background (CRB) have been extensively studied in the recent years (e.g. Gervasi et al. 2008; Singal et al. 2010; Vernstrom et al. 2011, 2014; Ysard & Lagache 2012; Condon et al. 2012). All these studies report that only a small fraction of this background (∼10–26%) can be accounted for by objects resolved in the deepest existing radio surveys. Thus, they conclude that if the CRB at 3.3 GHz is at the level reported by ARCADE2, it must originate from very faint radio sources still to be observed. In particular, Singal et al. (2010) speculate that these sources could have radio flux densities <10 μJy and be ordinary star-forming galaxies at $z > 1$ associated with an FRC that has evolved towards radio-loud (numerically lower) values. Such evolution of the FRC is qualitatively supported by our observations. However, quantitatively, the evolution of $q_{\rm FIR}$ required by Singal et al. (2010) is much larger than that observed here, i.e. $\Delta q_{\rm FIR} < -0.7$ instead of the observed $\Delta q_{\rm FIR} \sim -0.3$ at $z \sim 2$. From the total infrared luminosity density across $0 < z < 4$ inferred by Gruppioni et al. (2013; see also Magnelli et al. 2013) using *Herschel* observations[17], we can estimate the contribution of star-forming galaxies to the CRB at 3.3 GHz. Assuming $S_\nu \propto \nu^{-0.8}$ and $q_{\rm FIR} = 2.34$ across $0 < z < 4$, we find $\nu I_\nu^{\rm FRC} \approx 3.1 \times 10^{-5}\,{\rm nW\,m^{-2}\,sr^{-1}}$, i.e. 5.2% of the total CRB at 3.3 GHz. Instead, using $q_{\rm FIR}(z) = 2.35 \times (1+z)^{-0.12}$ at $0 < z < 2.3$ and $q_{\rm FIR}(z > 2) = q_{\rm FIR}(z = 2)$, we find $\nu I_\nu^{\rm FRC} \approx 4.5 \times 10^{-5}\,{\rm nW\,m^{-2}\,sr^{-1}}$, i.e. 7.6% of the total CRB at 3.3 GHz. Finally, using $q_{\rm FIR}(z) = 2.35 \times (1+z)^{-0.12}$ at $0 < z < 4$, we find $\nu I_\nu^{\rm FRC} \approx 4.6 \times 10^{-5}\,{\rm nW\,m^{-2}\,sr^{-1}}$, i.e. 7.7% of the total CRB at 3.3 GHz. Therefore, while the evolution of the FRC with redshift increases the resolved fraction of the CRB as measured by ARCADE2, it cannot entirely explain its origin. We conclude that if the CRB is at the level reported here, the contribution of star-forming galaxies that obey the FRC is at most ∼10% (taking into account a dispersion of the FRC of 0.3). However, note that a proper treatment of outliers of the FRC should be performed in order to estimate the entire contribution of infrared sources to the CRB.

We also estimate the contribution of X-ray AGNs to the CRB at 3.3 GHz. In each of our redshift bin, we measure the mean 1.4 GHz flux density of X-ray AGNs using our stacking analysis. Then, to obtain the 1.4 GHz radio background of X-ray AGNs, we multiply this mean radio flux by the density of X-ray AGNs detected in our GOODS-N/S samples (i.e. fields with the deepest X-ray datasets). Finally, we convert this 1.4 GHz radio background into a 3.3-GHz radio background assuming a radio spectral index of X-ray AGNs in the range [0.5−1.0]. We found that X-ray AGNs have $\nu I_\nu^{\text{X-ray AGNs}} \approx 11.0\,(7.2) \times 10^{-6}\,{\rm nW\,m^{-2}\,sr^{-1}}$, assuming a radio spectral index of 0.5 (1.0). This corresponds to only ∼1.9% (1.2%) of the total CRB measured by ARCADE2 at 3.3 GHz.

6. Summary

In this paper we study the evolution of the FRC and radio spectral index ($\alpha_{610\,\rm MHz}^{1.4\,\rm GHz}$) across the SFR–$M_*$ plane and up to $z \sim 2$. We use the deepest FIR-*Herschel*, 1.4 GHz (VLA) and 610 MHz (GMRT) observations available for the GOODS-N, GOODS-S, ECDFS and COSMOS fields. Infrared luminosities are inferred using the stacked PACS/SPIRE FIR photometry for each SFR–M_*–z bin. Radio luminosities and radio spectral indices are derived using their stacked 1.4 GHz and 610 MHz flux densities. Using this methodology, we are able to overcome most of the biases affecting previous studies on the FRC. Selection biases are overcome by the use of a complete stellar-mass-selected ($M_* \gtrsim 10^{10}\,M_\odot$) sample of star-forming galaxies at $0 < z < 2.3$. Observational biases, introduced by sparse coverage of the FIR and radio spectra, are overcome by the use of multi-wavelength FIR and radio observations. Our results, which are valid for all star-forming galaxies with $M_* > 10^{10}\,M_\odot$,

[17] Note that the cosmic infrared background derived here from the total infrared luminosity density across $0 < z < 4$ is of $25.5\,{\rm nW\,m^{-2}\,sr^{-1}}$, in agreement with estimates of Dole et al. (2006) and Béthermin et al. (2012).

$\Delta\log(SSFR)_{\rm MS} > -0.3$ and $0 < z < 2.3$, can be summarised as follows:

1. The radio spectral index, $\alpha^{1.4\,\rm GHz}_{610\,\rm MHz}$, does not evolve significantly with the distance of a galaxy with respect to the MS (i.e. $\Delta\log(SSFR)_{\rm MS}$) nor with redshift. Instead, $\alpha^{1.4\,\rm GHz}_{610\,\rm MHz}$ remains relatively constant across the SFR–M_*–z parameter space, consistent with a canonical value of 0.8. This results suggests that the radio spectra of the bulk of the high-redshift star-forming galaxy population is dominated by non-thermal optically thin synchrotron emission, well described by a power-law function, $S_\nu \propto \nu^{-0.8}$, across the range of rest-frequencies probed here, 610 MHz $< \nu_{\rm rest} <$ 4.2 GHz.
2. A relatively constant radio spectral index from normal star-forming galaxies ($\Delta\log(SSFR)_{\rm MS} \gtrsim 0$) to starbursts ($\Delta\log(SSFR)_{\rm MS} \gtrsim 1$) is surprising in light of local observations where the radio spectra of ULIRGs are significantly flatter ($\alpha \sim 0.5$) than those of spiral galaxies ($\alpha \sim 0.8$; Condon et al. 1991; Clemens et al. 2008). However, the observation of relatively steep radio spectra in high-redshift starbursts is also supported by results from Ibar et al. (2009) and Thomson et al. (2014) who found $\alpha \sim 0.8$ for samples of individually detected high-redshift SMGs. The combination of these results suggests that most high-redshift starbursts have different ISM properties (e.g. magnetic field strength, gas densities, $\Sigma_{\rm SFR}$, ...) than their local counterparts. Alternatively, it could suggest that, as advocated by Condon et al. (1991), the flatter radio spectrum of local starbursts is due to free-free absorption, less relevant at the higher rest-frequencies probed at high redshift.
3. The FRC does not evolve significantly with $\Delta\log(SSFR)_{\rm MS}$, though the presence of a weak positive trend, as observed in one of our redshift bin (i.e. $\Delta[q_{\rm FIR}]/\Delta[\Delta\log(SSFR)_{\rm MS}] = 0.22 \pm 0.07$ at $0.5 < z < 0.8$), cannot be firmly ruled out using our dataset.
4. The FRC evolves with redshift as $q_{\rm FIR}(z) = (2.35 \pm 0.08) \times (1+z)^{-0.12\pm0.04}$. This redshift evolution of the FRC is consistent with previous findings from the literature, though most favoured a non-evolving FRC because high-redshift measurements were within its local 1σ dispersion, $q_{\rm FIR}(z \approx 0) = 2.34 \pm 0.26$ (Yun et al. 2001).
5. The fact that the FRC still holds at high redshift, albeit with some moderate evolution, suggests that IC cooling of CR electrons and protons off photons from the CMB ($U_{\rm CMB} \propto (1+z)^4$) does not yet dominate over synchrotron cooling at $z \sim 2$. The redshift evolution of the FRC suggests that the ISM properties (e.g. magnetic field strength, gas densities, $\Sigma_{\rm SFR}$, ...) of star-forming galaxies evolve between $z \sim 0$ and $z \sim 2$.

A decrease in $q_{\rm FIR}$ with redshift was expected by some of the most up-to-date theoretical models of the FRC, e.g. L10, LT10 and S13. Such evolution is expected because $\Sigma_{\rm SFR}$ and $\rho_{\rm gas}$, which control in part the normalisation of the FRC, are known to evolve significantly with redshift. While the model of S13 seems to over-estimate the decrease in $q_{\rm FIR}$ with redshift, the bulk of the high-redshift star-forming galaxy population follows the expectations of LT10 by evolving smoothly from their normal-to-compact starbursts track at $z \sim 0$ to their normal-to-puffy starbursts track at $z \sim 2$. This suggests that MS galaxies have a constant CR scale height of ~1 kpc across $0 < z < 2.3$ and that their $q^{\rm MS}_{\rm FIR}$ decrease by 0.3 at $z \sim 2$ because their $\Sigma_{\rm SFR}$ changes from $\Sigma_{\rm SFR} \sim 0.02\,M_\odot\,{\rm kpc}^{-2}\,{\rm yr}^{-1}$ to $\Sigma_{\rm SFR} \sim 1\,M_\odot\,{\rm kpc}^{-2}\,{\rm yr}^{-1}$ in this redshift range. A constant CR scale height for MS galaxies is consistent with the current interpretation of the MS of star formation. Indeed, despite their extreme $\Sigma_{\rm SFR}$, high-redshift MS galaxies have the physical properties of local normal star-forming galaxies (e.g. Wuyts et al. 2011b; Elbaz et al. 2011; Magnelli et al. 2012b, 2014). In addition, our results suggests that most starbursts have a CR scale height of ~0.1 kpc at $z \sim 0$ and of ~1 kpc at $z \sim 2$. This translates into a smooth decrease in $q_{\rm FIR}$ by 0.3 at $z \sim 2$, as starbursts move from the compact starburst to the puffy starburst predictions of LT10. Nevertheless, this vision of an homogeneous high-redshift starburst population, constituted only of puffy starbursts, is compromised by the possibility of a weak $q_{\rm FIR} - \Delta\log(SSFR)_{\rm MS}$ correlation, combined with a larger dispersion in $q_{\rm FIR}$ at high $\Delta\log(SSFR)_{\rm MS}$. These latter observations support a scenario in which a non-negligible number of high-redshift starbursts are compact.

Our results have important implications for studies relying on the local FRC. For example, SFRs of high-redshift galaxies determined via radio observations will be lower than predicted by the local FRC. However, because $q_{\rm FIR}$ is still within its local 1σ dispersion at $z \sim 2$, uncertainties on previous SFR estimates should capture this evolution.

It has been postulated in the past that the CRB detected by ARCADE2 at 3.3 GHz could be dominated by $z > 1$ star-forming galaxies obeying an evolved, radio-loud FRC (e.g. Singal et al. 2010). However, we find that star-forming galaxies responsible for the CIB contribute at most ~10% of the CRB, even after having accounted for the evolution of the FRC observed here.

Acknowledgements. We thank the anonymous referee for suggestions which greatly enhanced this work. PACS has been developed by a consortium of institutes led by MPE (Germany) and including UVIE (Austria); KU Leuven, CSL, IMEC (Belgium); CEA, LAM (France); MPIA (Germany); INAF-IFSI/OAA/OAP/OAT, LENS, SISSA (Italy); IAC (Spain). This development has been supported by the funding agencies BMVIT (Austria), ESA-PRODEX (Belgium), CEA/CNES (France), DLR (Germany), ASI/INAF (Italy), and CICYT/MCYT (Spain). SPIRE has been developed by a consortium of institutes led by Cardiff University (UK) and including University of Lethbridge (Canada), NAOC (China), CEA, LAM (France), IFSI, University of Padua (Italy), IAC (Spain), Stockholm Observatory (Sweden), Imperial College London, RAL, UCL-MSSL, UKATC, University of Sussex (UK), Caltech, JPL, NHSC, University of Colorado (USA). This development has been supported by national funding agencies: CSA (Canada); NAOC (China); CEA, CNES, CNRS (France); ASI (Italy); MCINN (Spain); SNSB (Sweden); STFC, UKSA (UK); and NASA (USA). Support for BM was provided by the DFG priority programme 1573 The physics of the interstellar medium. R.J.I. acknowledges support from the European Research Council in the form of Advanced Grant, COSMICISM. E.I. acknowledges funding from CONICYT/FONDECYT postdoctoral project N°:3130504. F.B. and A.K. acknowledge support by the Collaborative Research Council 956, sub-project A1, funded by the Deutsche Forschungsgemeinschaft (DFG).

References

Alexander, D. M., Bauer, F. E., Brandt, W. N., et al. 2003, AJ, 125, 383
Appleton, P. N., Fadda, D. T., Marleau, F. R., et al. 2004, ApJS, 154, 147
Balestra, I., Mainieri, V., Popesso, P., et al. 2010, A&A, 512, A12
Barger, A. J., Cowie, L. L., & Wang, W.-H. 2008, ApJ, 689, 687
Bauer, F. E., Alexander, D. M., Brandt, W. N., et al. 2004, AJ, 128, 2048
Beck, R., & Golla, G. 1988, A&A, 191, L9
Bell, E. F., McIntosh, D. H., Katz, N., & Weinberg, M. D. 2003, ApJS, 149, 289
Béthermin, M., Le Floc'h, E., Ilbert, O., et al. 2012, A&A, 542, A58
Bicay, M. D., & Helou, G. 1990, ApJ, 362, 59
Biggs, A. D., & Ivison, R. J. 2008, MNRAS, 385, 893
Bourne, N., Dunne, L., Ivison, R. J., et al. 2011, MNRAS, 410, 1155
Brammer, G. B., van Dokkum, P. G., & Coppi, P. 2008, ApJ, 686, 1503
Brinchmann, J., Charlot, S., White, S. D. M., et al. 2004, MNRAS, 351, 1151
Bruzual, G., & Charlot, S. 2003, MNRAS, 344, 1000
Buat, V., Iglesias-Páramo, J., Seibert, M., et al. 2005, ApJ, 619, L51
Cappelluti, N., Brusa, M., Hasinger, G., et al. 2009, A&A, 497, 635
Cardamone, C. N., van Dokkum, P. G., Urry, C. M., et al. 2010, ApJS, 189, 270
Carilli, C. L., & Yun, M. S. 1999, ApJ, 513, L13

Chabrier, G. 2003, ApJ, 586, L133
Chapman, S. C., Blain, A. W., Smail, I., & Ivison, R. J. 2005, ApJ, 622, 772
Chary, R., & Elbaz, D. 2001, ApJ, 556, 562
Cimatti, A., Daddi, E., Mignoli, M., et al. 2002, A&A, 381, L68
Cimatti, A., Cassata, P., Pozzetti, L., et al. 2008, A&A, 482, 21
Clemens, M. S., Vega, O., Bressan, A., et al. 2008, A&A, 477, 95
Cohen, J. G., Hogg, D. W., Blandford, R., et al. 2000, ApJ, 538, 29
Cohen, A. S., Röttgering, H. J. A., Jarvis, M. J., Kassim, N. E., & Lazio, T. J. W. 2004, ApJS, 150, 417
Condon, J. J. 1992, ARA&A, 30, 575
Condon, J. J., Huang, Z.-P., Yin, Q. F., & Thuan, T. X. 1991, ApJ, 378, 65
Condon, J. J., Cotton, W. D., Fomalont, E. B., et al. 2012, ApJ, 758, 23
Cowie, L. L., Barger, A. J., Hu, E. M., Capak, P., & Songaila, A. 2004, AJ, 127, 3137
Cristiani, S., Appenzeller, I., Arnouts, S., et al. 2000, A&A, 359, 489
Croom, S. M., Smith, R. J., Boyle, B. J., et al. 2001, MNRAS, 322, L29
Daddi, E., Dickinson, M., Morrison, G., et al. 2007, ApJ, 670, 156
Dale, D. A., & Helou, G. 2002, ApJ, 576, 159
Dale, D. A., Helou, G., Contursi, A., Silbermann, N. A., & Kolhatkar, S. 2001, ApJ, 549, 215
De Breuck, C., van Breugel, W., Röttgering, H. J. A., & Miley, G. 2000, A&AS, 143, 303
de Jong, T., Klein, U., Wielebinski, R., & Wunderlich, E. 1985, A&A, 147, L6
Del Moro, A., Alexander, D. M., Mullaney, J. R., et al. 2013, A&A, 549, A59
Devlin, M. J., Ade, P. A. R., Aretxaga, I., et al. 2009, Nature, 458, 737
Dole, H., Lagache, G., Puget, J.-L., et al. 2006, A&A, 451, 417
Donley, J. L., Rieke, G. H., Rigby, J. R., & Pérez-González, P. G. 2005, ApJ, 634, 169
Donley, J. L., Koekemoer, A. M., Brusa, M., et al. 2012, ApJ, 748, 142
Dumas, G., Schinnerer, E., Tabatabaei, F. S., et al. 2011, AJ, 141, 41
Dunne, L., Ivison, R. J., Maddox, S., et al. 2009, MNRAS, 394, 3
Elbaz, D., Daddi, E., Le Borgne, D., et al. 2007, A&A, 468, 33
Elbaz, D., Dickinson, M., Hwang, H. S., et al. 2011, A&A, 533, A119
Farrah, D., Lonsdale, C. J., Weedman, D. W., et al. 2008, ApJ, 677, 957
Fixsen, D. J., Kogut, A., Levin, S., et al. 2011, ApJ, 734, 5
Förster Schreiber, N. M., Genzel, R., Bouché, N., et al. 2009, ApJ, 706, 1364
Gabasch, A., Goranova, Y., Hopp, U., Noll, S., & Pannella, M. 2008, MNRAS, 383, 1319
Gervasi, M., Tartari, A., Zannoni, M., Boella, G., & Sironi, G. 2008, ApJ, 682, 223
Griffin, M. J., Abergel, A., Abreu, A., et al. 2010, A&A, 518, L3
Gruppioni, C., Pozzi, F., Rodighiero, G., et al. 2013, MNRAS, 432, 23
Hasinger, G., Miyaji, T., & Schmidt, M. 2005, A&A, 441, 417
Helou, G., Soifer, B. T., & Rowan-Robinson, M. 1985, ApJ, 298, L7
Helou, G., Khan, I. R., Malek, L., & Boehmer, L. 1988, ApJS, 68, 151
Huynh, M. T., Frayer, D. T., Mobasher, B., et al. 2007, ApJ, 667, L9
Ibar, E., Cirasuolo, M., Ivison, R., et al. 2008, MNRAS, 386, 953
Ibar, E., Ivison, R. J., Biggs, A. D., et al. 2009, MNRAS, 397, 281
Ibar, E., Ivison, R. J., Best, P. N., et al. 2010, MNRAS, 401, L53
Ilbert, O., Capak, P., Salvato, M., et al. 2009, ApJ, 690, 1236
Ivison, R. J., Alexander, D. M., Biggs, A. D., et al. 2010a, MNRAS, 402, 245
Ivison, R. J., Magnelli, B., Ibar, E., et al. 2010b, A&A, 518, L31
Ivison, R. J., Swinbank, A. M., Swinyard, B., et al. 2010c, A&A, 518, L35
Ivison, R. J., Papadopoulos, P. P., Smail, I., et al. 2011, MNRAS, 412, 1913
Jackson, C. A., & Wall, J. V. 1999, MNRAS, 304, 160
Karim, A., Schinnerer, E., Martínez-Sansigre, A., et al. 2011, ApJ, 730, 61
Kennicutt, Jr., R. C. 1998, ARA&A, 36, 189
Kriek, M., van Dokkum, P. G., Franx, M., et al. 2008, ApJ, 677, 219
Kriek, M., van Dokkum, P. G., Labbé, I., et al. 2009, ApJ, 700, 221
Lacki, B. C., & Thompson, T. A. 2010, ApJ, 717, 196
Lacki, B. C., Thompson, T. A., & Quataert, E. 2010, ApJ, 717, 1
Lacy, M., Petric, A. O., Sajina, A., et al. 2007, AJ, 133, 186
Le Fèvre, O., Vettolani, G., Paltani, S., et al. 2004, A&A, 428, 1043
Le Floc'h, E., Aussel, H., Ilbert, O., et al. 2009, ApJ, 703, 222
Lehmer, B. D., Brandt, W. N., Alexander, D. M., et al. 2005, ApJS, 161, 21
Lilly, S. J., Le Brun, V., Maier, C., et al. 2009, ApJS, 184, 218
Luo, B., Bauer, F. E., Brandt, W. N., et al. 2008, ApJS, 179, 19
Lutz, D., Poglitsch, A., Altieri, B., et al. 2011, A&A, 532, A90
Magdis, G. E., Elbaz, D., Dickinson, M., et al. 2011, A&A, 534, A15
Magnelli, B., Elbaz, D., Chary, R. R., et al. 2009, A&A, 496, 57
Magnelli, B., Elbaz, D., Chary, R. R., et al. 2011, A&A, 528, A35
Magnelli, B., Lutz, D., Santini, P., et al. 2012a, A&A, 539, A155
Magnelli, B., Saintonge, A., Lutz, D., et al. 2012b, A&A, 548, A22
Magnelli, B., Popesso, P., Berta, S., et al. 2013, A&A, 553, A132
Magnelli, B., Lutz, D., Saintonge, A., et al. 2014, A&A, 561, A86
Mancini, C., Förster Schreiber, N. M., Renzini, A., et al. 2011, ApJ, 743, 86
Mignoli, M., Cimatti, A., Zamorani, G., et al. 2005, A&A, 437, 883
Miller, N. A., Fomalont, E. B., Kellermann, K. I., et al. 2008, ApJS, 179, 114
Miller, N. A., Bonzini, M., Fomalont, E. B., et al. 2013, ApJS, 205, 13
Morrison, G. E., Owen, F. N., Dickinson, M., Ivison, R. J., & Ibar, E. 2010, ApJS, 188, 178
Murphy, E. J. 2009, ApJ, 706, 482
Murphy, E. J. 2013, ApJ, 777, 58
Murphy, E. J., Helou, G., Kenney, J. D. P., Armus, L., & Braun, R. 2008, ApJ, 678, 828
Murphy, E. J., Chary, R.-R., Alexander, D. M., et al. 2009, ApJ, 698, 1380
Murphy, E. J., Condon, J. J., Schinnerer, E., et al. 2011, ApJ, 737, 67
Newman, S. F., Genzel, R., Förster Schreiber, N. M., et al. 2013, ApJ, 767, 104
Niklas, S., & Beck, R. 1997, A&A, 320, 54
Noeske, K. G., Weiner, B. J., Faber, S. M., et al. 2007, ApJ, 660, L43
Nordon, R., Lutz, D., Genzel, R., et al. 2012, ApJ, 745, 182
Oliver, S., Frost, M., Farrah, D., et al. 2010, MNRAS, 405, 2279
Oliver, S. J., Bock, J., Altieri, B., et al. 2012, MNRAS, 424, 1614
Pannella, M., Carilli, C. L., Daddi, E., et al. 2009, ApJ, 698, L116
Park, S. Q., Barmby, P., Fazio, G. G., et al. 2008, ApJ, 678, 744
Pilbratt, G. L., Riedinger, J. R., Passvogel, T., et al. 2010, A&A, 518, L1
Poglitsch, A., Waelkens, C., Geis, N., et al. 2010, A&A, 518, L2
Reddy, N. A., Steidel, C. C., Fadda, D., et al. 2006, ApJ, 644, 792
Rieke, G. H., Young, E. T., Engelbracht, C. W., et al. 2004, ApJS, 154, 25
Rodighiero, G., Cimatti, A., Gruppioni, C., et al. 2010, A&A, 518, L25
Rodighiero, G., Daddi, E., Baronchelli, I., et al. 2011, ApJ, 739, L40
Roseboom, I. G., Oliver, S. J., Kunz, M., et al. 2010, MNRAS, 409, 48
Sargent, M. T., Schinnerer, E., Murphy, E., et al. 2010, ApJS, 186, 341
Schiminovich, D., Wyder, T. K., Martin, D. C., et al. 2007, ApJS, 173, 315
Schinnerer, E., Carilli, C. L., Scoville, N. Z., et al. 2004, AJ, 128, 1974
Schinnerer, E., Smolčić, V., Carilli, C. L., et al. 2007, ApJS, 172, 46
Schinnerer, E., Sargent, M. T., Bondi, M., et al. 2010, ApJS, 188, 384
Schleicher, D. R. G., & Beck, R. 2013, A&A, 556, A142
Seiffert, M., Fixsen, D. J., Kogut, A., et al. 2011, ApJ, 734, 6
Seymour, N., Huynh, M., Dwelly, T., et al. 2009, MNRAS, 398, 1573
Singal, J., Stawarz, Ł., Lawrence, A., & Petrosian, V. 2010, MNRAS, 409, 1172
Smail, I., Ivison, R. J., & Blain, A. W. 1997, ApJ, 490, L5
Stern, D., Eisenhardt, P., Gorjian, V., et al. 2005, ApJ, 631, 163
Szokoly, G. P., Bergeron, J., Hasinger, G., et al. 2004, ApJS, 155, 271
Tabatabaei, F. S., Berkhuijsen, E. M., Frick, P., Beck, R., & Schinnerer, E. 2013a, A&A, 557, A129
Tabatabaei, F. S., Schinnerer, E., Murphy, E. J., et al. 2013b, A&A, 552, A19
Tacconi, L. J., Neri, R., Chapman, S. C., et al. 2006, ApJ, 640, 228
Thomson, A. P., Ivison, R. J., Simpson, J. M., et al. 2014, MNRAS, 442, 577
Treister, E., Virani, S., Gawiser, E., et al. 2009, ApJ, 693, 1713
van der Wel, A., Franx, M., van Dokkum, P. G., & Rix, H.-W. 2004, ApJ, 601, L5
Vanzella, E., Cristiani, S., Dickinson, M., et al. 2006, A&A, 454, 423
Vanzella, E., Cristiani, S., Dickinson, M., et al. 2008, A&A, 478, 83
Vernstrom, T., Scott, D., & Wall, J. V. 2011, MNRAS, 415, 3641
Vernstrom, T., Scott, D., Wall, J. V., et al. 2014, MNRAS, 440, 2791
Völk, H. J. 1989, A&A, 218, 67
Wall, J. V., Jackson, C. A., Shaver, P. A., Hook, I. M., & Kellermann, K. I. 2005, A&A, 434, 133
Whitaker, K. E., van Dokkum, P. G., Brammer, G., & Franx, M. 2012, ApJ, 754, L29
Wirth, G. D., Willmer, C. N. A., Amico, P., et al. 2004, AJ, 127, 3121
Wuyts, S., Förster Schreiber, N. M., Lutz, D., et al. 2011a, ApJ, 738, 106
Wuyts, S., Förster Schreiber, N. M., van der Wel, A., et al. 2011b, ApJ, 742, 96
Ysard, N., & Lagache, G. 2012, A&A, 547, A53
Yun, M. S., Reddy, N. A., & Condon, J. J. 2001, ApJ, 554, 803